REPUBLIQUE DU CAMEROUN
Paix-Travail-Patrie
****
UNIVERSITE DE YAOUNDE I
****
CENTRE DE RECHERCHE ET DE
FORMATION
DOCTORALE EN SCIENCES,
TECHNOLOGIES
ET GEOSCIENCES
****
UNITE DE RECHERCHE ET DE FORMATION
DOCTORALE EN PHYSIQUES ET
APPLICATIONS
****
B.P 812 Yaoundé
Email: crfd_stg@uy1.uninet.cm

REPUBLIC OF CAMEROON
Peace-Work-Fatherland
****
THE UNIVERSITY OF YAOUNDE I
****
POSTGRADUATE SCHOOL OF
SCIENCES,
TECHNOLOGY AND GEOSCIENCES
****
RESEARCH AND POSTGRADUATE
TRAINING UNIT FOR PHYSICS AND
APPLICATIONS
****
P.O. Box 812 Yaoundé
Email: crfd_stg@uy1.uninet.cm

MICROCONTROLLER AND ANALOG STUDY OF THE SYNCHRONIZATION OF COUPLED VAN DER POL OSCILLATORS

Thesis submitted and defended in partial fulfillment of the requirements for the awards

of a Doctor of Philosophy (Ph.D) degree in Physics

Option: Fundamental Mechanics and Complex Systems

By

THEPI SIEWE Raoul

Registration Number: 08W0637

Master in Physics

Under the supervision of

WOAFO Paul

Professor

©Year 2020

UNIVERSITÉ DE YAOUNDÉ I
UNIVERSITY OF YAOUNDE I

FACULTÉ DES SCIENCES
FACULTY OF SCIENCE

DÉPARTEMENT DE PHYSIQUE
DEPARTMENT OF PHYSICS

ATTESTATION DE CORRECTION DE LA THÈSE DE

DOCTORAT/Ph.D

Nous, Professeur **EYEBE FOUDA Jean Sire** et Professeur **ESSIMBI ZOBO Bernard** respectivement Examinateur et Président du jury de la Thèse de Doctorat/Ph.D de Monsieur **THEPI SIEWE Raoul**, Matricule **08W0637**, préparée sous la supervision du Professeur **WOAFO Paul**, intitulée : « **MICROCONTROLLER AND ANALOG STUDY OF THE SYNCHRONIZATION OF COUPLED VAN DER POL OSCILLATORS** », soutenue le **Jeudi, 5 Novembre 2020**, en vue de l'obtention du grade de Docteur/Ph.D en Physique, Spécialité **Mécanique, Matériaux et Structures,** Option **Mécanique Fondamentale et Systèmes Complexes,** attestons que toutes les corrections demandées par le jury de soutenance ont été effectuées.

En foi de quoi, la présente attestation lui est délivrée pour servir et valoir ce que de droit.

Fait à Yaoundé le ......**2 7 NOV 2020**...............

Examinateur

Prof. EYEBE FOUDA Jean Sire

Le Chef de Département de Physique

Le Chef de Département

Prof. NDJAKA Jean-Marie Bienvenu

Le Président du jury

Prof. ESSIMBI ZOBO BERNARD

Dedications

o To God for all the power and strength that he gives me every day of my life;

o To my parents: Mrs. Pouatchui Cecile and Mr. SIEWE Jean Paul for all their patience, continuous encouragements and advices;

o To my sisters and brothers: Mr. EWOLO Hervé, late Mrs. MONGOUE Diane, Mr. KAMAKO Landry, Mr. TCHEULATCHUI Jean-Baptiste, Mrs. NGUENKAM Joelle, Mrs. SEUMTCHA Carine, Mrs. YAMACHI Leonie, Mrs. NGOPTCHOKO Pélagie, Mrs. SIEWE Bernice, Mrs. TCHASSI Olive, Mr. WONTCHEU Steve, Mr. WEILADJI Fred and Mr. TCHOBE Arsène for their moral supports;

o Particularly to Mrs. KAKLIEU DOUANOU Darole, Mrs. SIEWE THEPI Nesline Godwin and Mrs. SIAKAM THEPI Goodness Orchelle for their moral support.

Acknowledgements

I would like to thank respectively:

Professor WOAFO Paul, my supervisor for the trust, relationship, guidance and support during the years of my graduate study. Professor, from my works of Master up to now, you have grown in me good qualities (humanistic, entrepreneurship and scientific) which, I hope, will make me a great man. Thanks one more.

Professor KENFACK JIOTSA Aurelien to whom I would like to express my acknowledgments for his open mind and willing to listen and discuss about almost any problem during my Master.

Professor NDJAKA Jean-Marie Bienvenu, Head of Department of Physics, Faculty of Science, UYI and the teaching staff of this department for their valuable teaching and their fruitful advices.

Professor KOFANE Timoléon Crépin whose impulse to nonlinear physics in Cameroon for the last two decades has been too beneficial to me.

Professor NANA NBENDJO Blaise Roméo, I would like to express my acknowledgments for his open mind lesson teaching encouragements during my Master and thesis.

Postgraduate school specially the subdivision of sciences, technology and geosciences which gave me the opportunity to conduct this doctoral training.

I acknowledge in advance the scientists for accepting to examine this pre-thesis: the President of jury Professor **ESSIMBI ZOBO Bernard** of University of Yaoundé 1; the members of jury namely Professors **TCHAWOUA Clément, EYEBE FOUDA Jean Sire** and **KENFACK JIOTSA Aurélien** of University of Yaoundé 1.

Dr. NANA Bonaventure, Dr. NOUBISSIÉ Samuel and late Dr. MBOUSSI NKOMIDIO Aïssatou for the fruitful interactions since my academic years of Master until now.

Dr. TALLA Francis for his fruitful interactions and discussions during the experimental parts of my thesis.

Table of contents

List of abbreviations

A/D: Analogical/Digital

ADC: Analog **D**igital **C**onverter

CCP: Capture **C**ompare **P**eripherals

CPU: Central **P**rocessing **U**nit

DDE: **D**elayed **D**ifferential **E**quation

DE: **D**ifferential **E**quation

EEPROM: Electrically **E**rasable **P**rogram **R**ead **O**nly **M**emory

IIC: Inter-**I**ntegrated **C**ircuit

I/O: Input /**O**utput

MaEMS: **M**acro **E**lectro-**M**echanical **S**ystem

MCU: **M**icro-**C**ontroller **U**nit

ODE: Ordinary **D**ifferential **E**quation

OP-AMP: **O**perational **A**mplifier

PMW: Pulse **M**odulator **W**idth

PIC: Peripheral **I**nterface **C**enter

RAM: **R**andom **A**ccess **M**emory

RK: Runge-**K**utta

ROM: Read **O**nly **M**emory

SFR: Serial **F**unction **R**andom

μ**C**: microcontroller

USART: Universal **S**ynchronous **A**synchronous **R**eceiver-**T**ransmitter

USB: Universal **S**erial **B**us

WDT: Width **D**igital **T**ransfer

List of figures

Abstract

This thesis deals with the analog electronic and microcontroller study of the synchronization of coupled Van der Pol oscillators and application to the command of electromechanical systems. Polynomial and delay unidirectional couplings are considered. The intervals of coupling coefficients and delay leading to synchronization are determined experimentally using analog electronic circuits. Three cases are considered: autonomous Van der Pol oscillators, sinusoidally excited Van der Pol oscillators in the chaotic state and Van der Pol oscillators with two slowly sinusoidal excitations delivering periodic patterns of periodic pulses. It is found that increasing the degree of the polynomial coupling reduces the intervals of coupling coefficients leading to synchronization and the delay affects the coupling intervals in a periodic way. The experimental results agree qualitatively with the results of the mathematical (according to the Floquet theory) and the numerical investigations. We conduct the micro controller implementation of the synchronization of two Van der Pol oscillators submitted to disturbances of the pulse-like type. Three coupling schemes are used: the classical linear proportional coupling, a power order n coupling and an adaptive coupling. After obtaining the coupling coefficients for synchronization through numerical simulation, the micro controller implementation is carried out using simulation based on Euler algorithm. Qualitative agreement is found between both simulation strategies. Based on the microcontroller studies, we fabricate a simple generator of self-sustained, chaotic oscillator and special signals which can be used in laboratories for experimental works.

Keywords: Van der Pol oscillator, synchronization, control, experimental studies, pulse signal patterns, microcontroller, generator.

Résumé

Cette thèse porte sur l'étude par simulation analogique et par microcontrôleurs de la synchronisation des oscillateurs de Van der Pol couplés. Des couplages unidirectionnels, polynomiaux et à retard sont considérés. Les intervalles de coefficients de couplage et de délai menant à la synchronisation sont déterminés expérimentalement à l'aide de circuits électroniques analogiques. Trois cas sont considérés: les oscillateurs de Van der Pol autonomes, les oscillateurs de Van der Pol excités et à l'état chaotique et les oscillateurs de Van der Pol soumis à l'excitation de deux forces lentes et sinusoïdales délivrant des motifs d'impulsions périodiques. On constate que l'augmentation du degré de couplage polynomial réduit les intervalles de coefficients de couplage conduisant à la synchronisation et que le retard affecte les intervalles de couplage d'une manière périodique. Les résultats expérimentaux s'accordent qualitativement bien avec les résultats de l'investigation mathématique (selon la théorie de Floquet) et numérique. Nous étudions la mise en œuvre par microcontrôleur de la synchronisation de deux oscillateurs de Van der Pol soumis à des perturbations de type pulsées. Trois schémas de couplage sont utilisés: le couplage proportionnel linéaire, le couplage de puissance n et le couplage adaptatif. Après avoir obtenu les coefficients de couplage pour la synchronisation par simulation numérique, l'étude par microcontrôleur est effectuée à l'aide d'une simulation basée sur l'algorithme d'Euler. Un accord qualitatif est trouvé entre les deux stratégies de simulation. Sur la base des études avec les microcontrôleurs, nous fabriquons un générateur de signaux autoentretenus, chaotiques et spéciaux qui peuvent être utilisés dans des laboratoires pour les travaux pratiques.

Mots clés: Oscillateur de Van der Pol, synchronisation, contrôle, études expérimentales, paquets de signaux pulsés, microcontrôleur, générateur

General Introduction

After some decades of theoretical and experimental studies on nonlinear phenomena, several researchers have focused their attention on the problems related to the synchronization and control in networks of identical and non identical nonlinear oscillators. Today, researchers are now engaged towards the applications of nonlinear behaviours (such as multi-periodic, quasi-periodic oscillations and chaos) in different fields using different coupling schemes [1-8], different mathematical methods, numerical quantifiers and experimental methods. In Ref. [9], the authors studied theoretically the synchronization of two Van der Pol oscillators in the autonomous and non-autonomous states and linked by a linear coupling. They applied the Floquet theory approach on the variational equation describing the time dynamics of the deviation between the slave and master systems and came out with analytical conditions for synchronization and synchronization time. An interesting agreement was found between the analytical results and those obtained from the numerical simulation. But no experimental investigation was undertaken. An extension was conducted in Refs. [10-12] in case of a ring of two, four coupled Van der Pol oscillators with linear mutual (diffusive) coupling without delay. Both the theoretical and experimental studies were conducted in order to find the parameter leading to synchronization.

In some cases, the coupling mechanism can lead to time delay which has strong impact on synchronization conditions [13-18]. For instance, in Refs. [13-15], it was established that the critical coupling coefficient leading to synchronization of linearly coupled nonlinear oscillators is a periodic function of the delay.

The work carried out in Ref. [9] presented some interesting results for the synchronization of two Van der Pol oscillators coupled in a master-slave configuration. One of the goals of the present work is to obtain experimentally the intervals of the coupling constants leading to synchronization of two Van der Pol oscillators considering in the first instance coupling of the polynomial form and coupling with delay, and in the second instance different excitation states of the Van der Pol oscillators (autonomous state, excited state generating chaos and excited state delivering patterns of periodic pulses).

The World technologies are moving to embedded systems. An embedded system is a computer system used for specific applications such as in robotics and control. These embedded systems are based on microcontrollers which are used in several applications in different fields [19 –24]. In recent years, the scientific community working on nonlinear dynamical systems had been interested in using microcontrollers to provide complex dynamics. For instance, the

implementation of a chaotic Lorenz oscillator into a simple low-cost microcontroller has been carried out in Ref. [25]. In the same line, the implementation of a novel robust transmission scheme for private digital communications using Arduino Uno board has been implemented in Refs. [26, 27] and other contributions appear in Refs. [28, 29]. The embedded technologies are thus new tools to master nonlinear dynamics (simulation and synchronization). **This will be used in this work to analyze the synchronization of two Van der Pol oscillators working in the regular regime, but subjected to perturbations which generate phase difference. Three types of control schemes are considered: the usual proportional coupling/control, the proportional coupling with law power, and an adaptive coupling scheme [30]. Although these coupling schemes are known in the literature, their implementation based on microcontroller appears interesting as they will lead to new embedded strategies for control and synchronization in nonlinear dynamics. Thanks to this new technology of embedded systems, we fabricate in this thesis an experimental self-sustained and chaotic generator.**

The present work is divided in three chapters. In chapter one, we briefly give some background on dynamics of Van der Pol oscillator, synchronization of Van der Pol oscillators, self-sustained, microcontrollers studies and finished by the objectives of the thesis. In chapter two, we present the mathematical formalisms, numerical simulation methods, analog construction of differential equations ended by microcontroller simulation of differential equations. Synchronization of Van der Pol oscillators: analog simulation results, synchronization/control results using microcontrollers, fabrication of self-sustained and chaotic signal generator are presented in Chapter three. We end with a general conclusion where the main results of the work are summarized and perspectives related to our present achievements are sketched.

Chapter I: Literature Review

I-1-   Introduction

The aim of this chapter is to give the general information on the synchronization of self-sustained oscillators, to recall some knowledge on embedded technologies and present some known results on self-sustained electromechanical systems. The objective of the thesis will be presented as limits of some results known in the literature. Section I-2 is devoted to the generalities on the dynamics of the Van der Pol oscillator. In Section I-3, an overview on synchronization of Van der Pol oscillators is given. Section I-4 deals with information on microcontrollers. Section I-5 will give the objectives of the thesis systems. Section I-6 will conclude the chapter.

I-2-   Dynamics and synchronization of Van der Pol oscillator

I-2-1-   The Van der Pol equation

During the first half of the 20th century, Balthazar van der Pol pioneered the fields of radio and telecommunications. In an era when these areas were much less advanced than they are today, vacuum tubes were used to control the flow of electricity in the circuitry of transmitters and receivers. In 1927, experiments with the vacuum tube triode circuit lead to the conclusion that all initial conditions (different to zero) converged to the same periodic orbit of finite amplitude. Since this behavior is different from the solutions of linear equations, Van der Pol proposed a nonlinear differential equation which was the first example of a non-linear self oscillating system [31].

$$\ddot{x} + \mu\left(x^2 - 1\right)\dot{x} + \omega_0^2 x = 0. \tag{1.1}$$

According to the different values of the damping non linear coefficient μ, Van der Pol oscillator presents two interesting behaviours as presented in the following subsection.

I-2-2-   Different behaviors of the Van der Pol oscillator

μ, is the main parameter characterizing different dynamics exhibited by the Van der Pol oscillator considering $\omega_0^2 = 1$.

○ When $\mu = 0$, there is no damping function and the equation becomes

$$\ddot{x} + \omega_0^2 x = 0. \tag{1.2}$$

This is a form of the simple harmonic oscillator, and there is always conservation of energy [31]. Figure 1.1 presents the phase plan exhibited by the oscillator in the situation of equation (1.2).
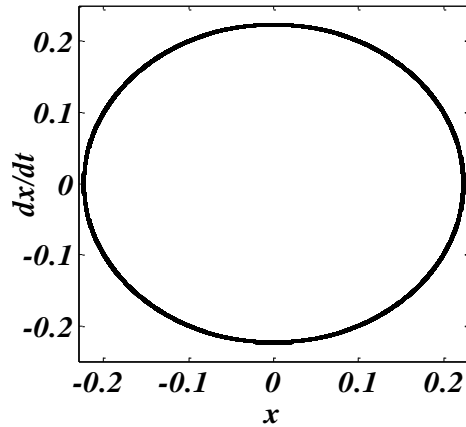
Figure 1.1: Phase portrait of the oscillator in the situation of $\mu = 0$.

o   When $\mu > 0$, two behaviors are presented.

➢ For $0 < \mu < 1$, the system will present a limit cycle. In that case, the Van der Pol oscillator exhibits the sinusoidal wave form as a sine function.

Figure 1.2 presents the phase portrait exhibited by the Van der Pol oscillator in this situation.
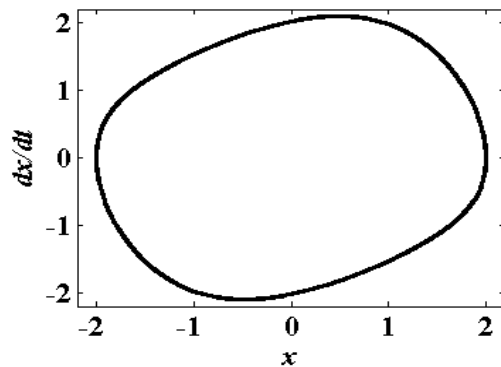
Figure 1.2: Phase portait of the oscillator in the situation of $\mu = 0.3$.

➢ For $\mu > 1$, the system presents another type of limit cycle showing relaxation oscillations.

Figure 1.3 shows the phase portrait exhibited by the Van der Pol oscillator in this situation.
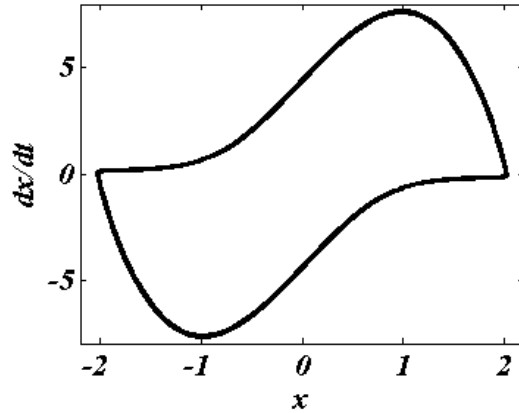
Figure 1.3: Phase portrait of the oscillator in the situation of $\mu = 5$.

Van der Pol commented on the importance of relaxation oscillations [32], which have become the cornerstones of geometric singular perturbation theory. Van der Pol went on to propose a version of two that includes a periodic forcing term [33].

$$\ddot{x} + \mu\left(x^2 - 1\right)\dot{x} + \omega_0^2 x = a\cos\left(\omega t\right).$$

(1.3)

Van der Pol and Van der Mark in their investigations of the oscillator behavior in the relaxation regime found that the subharmonic oscillations appeared during changes of natural frequency ω_0 of the system. The authors (in the September 1927 issue of the British journal Nature), noted the appearance of "irregular noise" before transition from one subharmonical regime to another. Moreover, they proposed an electrical model of the human heart consisting of three coupled relaxation oscillators [34].

According to these observations in the Van der Pol oscillator, Parlitz *et al.* found theoretically chaos in the forced oscillator as given in equation (1.3) by changing the values of a and ω [35]. Figure 1.4 presents the bifurcation diagram obtained in Ref. [35].
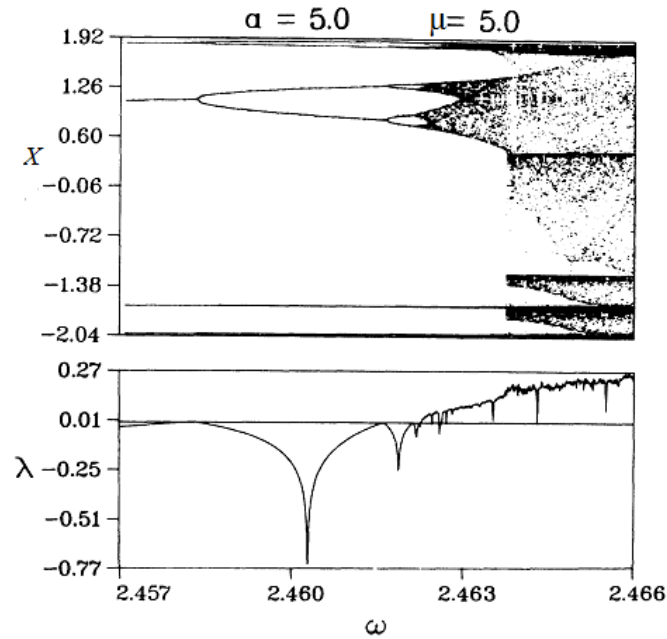
Figure 1.4: Enlargement of the bifurcation diagram and the corresponding evolution of the largest Lyapunov exponent λ and the winding number ω while $\omega_0 = 1$.

Figure 1.4 shows that for values of $\omega \in [2.457,\ 2.462]$, the oscillator present periodic behaviors and when $\omega \in [2.462,\ 2.466]$ the dynamics becomes chaotic. The largest Lyapunov exponent λ confirms clearly these situations.

I-2-3-   Applications of Van der Pol oscillators

The motivations for considering this oscillator are wide, including amongst others:

o   The Van der Pol oscillator is a single non-linear component for implementation of a sinusoidal oscillator which is widely used in electronic devices and communication systems.

o   The frequency of operation can vary from a few Hertz up to the microwave region (kilohertz), depending on the technology used.

o   The Van der Pol oscillator exhibits rich dynamical behavior like many other second-order forced oscillator configurations analyzed as mentioned [35-37].

o   According to its stability and different behaviors delivered (relaxation oscillations), the Van der Pol oscillator is used to model the human heart.

o In the field of neurophysiology, it is used to model the Gastric Mill Central Pattern Generator of the Lobster with a relaxation-oscillator network. The cell model is a generalization and extension of the Van der Pol relaxation oscillator equations [38].

o In seismology, the van der Pol equation has been used in the development of model of the interaction of two plates in a geological fault [39].

o In communication domain, excited Van der Pol oscillator produces chaos which is used to secure massages [40].

I-2-4- Synchronization of two Van der Pol oscillators

In 2002, Woafo and Kraenkel [9] consider the problem of stability and duration of the synchronization process between self-excited oscillators, both in their regular and chaotic states. Making use of the properties of Hill equation describing the deviation between the slave and the master, they derive the stability conditions and expressions of the synchronization time.

Synchronization of nonlinear oscillators both in their regular and chaotic states is presently one of the main research topics in the field of nonlinear science [41-48], since the pioneering work of Pecora and Carrol [1]. Woafo and Kraenkel considered the coupled Van der Pol oscillators given by the equation (1.4).

$$\begin{cases} \ddot{x} + \mu\left(x^2 - 1\right)\dot{x} + \omega_0^2 x = E\cos\left(\Omega t\right). \\ \ddot{u} + \mu\left(u^2 - 1\right) + \omega_0^2 u = E\cos\left(\Omega t\right) + k(u - x)H(t - T_0). \end{cases} \tag{1.4}$$

where k is the strength parameter for the synchronization process and E and Ω are respectively, the amplitude and frequency of the external excitation.

H is the Heaviside function defined as

$$H(t - T_0) = \begin{cases} 0 & si \quad t < T_0, \\ 1 & si \quad t \geq T_0, \end{cases} \tag{1.5}$$

Van der Pol oscillator is sensitive to initial conditions. When two such oscillators x and u with the same parameters are set into motion with different initial conditions, they evolve in the same limit cycle, but with different phases ϕ_1 and ϕ_2. One can thus synchronize by making the phases to be identical.

To carry out such an investigation, the authors introduce the variable z as given in equation (1.6)

$$z = u - x. \tag{1.6}$$

z here is the deviation between the master and slave. Assuming small μ, E and Ω taking equal to zero, it is found that z is described the following equation (1.7).

$$\ddot{z} + [2\lambda + F_1(\tau)]\dot{z} + G(\tau)z = 0. \tag{1.7}$$

where $F(\tau)$, $G(\tau)$, τ and λ are the functions and expressions given in Ref.[9].

To discuss further the stability process, equation (1.7) is rewritten in a standard form. For this purpose, one uses the transformation (1.8)

$$z = w\exp(-\lambda\tau)\exp\left(\frac{-1}{2}\int F(\tau)d\tau\right). \tag{1.8}$$

Inserting (1.8) into (1.7), it comes that w satisfies the following Hill's equation (1.9)

$$\ddot{w} + (a_0 + 2a_{1s}\sin 2\tau + 2a_{1c}\cos 2\tau + 2a_{1c}\cos 4\tau)w = 0. \tag{1.9}$$

where the coefficients a_i are given in Ref.[9].

From equation (1.9) and using the Whittaker method, it was established in Ref. [9] that the synchronization is achieved under the following conditions (1.10):

$$\left(a_0 - n^2\right)^2 + \left(2a_0 + n^2\right)\lambda^2 + \lambda^4 > a_n^2 \text{ with } n=1, 2. \tag{1.10}$$

Solving equation (1.10) has permitted to obtain the analytical results for small values of

μ ($\mu = 0.3$). The analytical domain of synchronization agrees well with the numerical simulation. For example it is found from the analytical consideration that the synchronization process is unstable for $k \in [-1.03, 0]$ while the numerical simulation gives $k \in [-0.39, 0]$.

Woafo and Kraenkel established analytically the mathematical expression of the synchronization time. This expression was confirmed by the results of the numerical simulation. Extending the study to the non-autonomous case, leading to chaos (for $\mu = E = 5$ and $\Omega \in [2.463, 2.466]$), it was found that intervals of synchronization alternate with the intervals where there is no synchronization.

I-2-5- Synchronization of many Van der Pol oscillators

In 2006, Enjieu *et al.* [49] examine the synchronization dynamics in a ring of four mutually coupled biological systems described by Van der Pol's coupled oscillators. The coupling parameters were not identical between the oscillators. The stability limits of the synchronization process were first evaluated without the influence of local injection using the eigenvalue properties and the fourth order Runge-Kutta algorithm. The effects of a locally injected trajectory on system stability limits in synchronized states were analyzed using numerical simulations. In both cases, the stability limits and the main dynamic states were reported on the stability maps in a plane depending on the coupling parameters to better distinguish the synchronization domains of the coupled oscillators [50-53].

During the same year, and following the same voice as Enjieu *et al.*, Nana *et al.* [10, 54-56] study different synchronization states in a ring of four Van der Pol oscillators coupled to each other. Stability analysis and numerical simulation were performed to determine the appropriate coupling parameters leading to high quality synchronization. The consequences of the differences in the parameters were also highlighted. The experimental realization is then used to show the existence of complete and partial synchronizations.

I-3- Information on microcontrollers

It was during 1970 and 1971 when Intel was working on inventing the world's first microprocessor, that **Gary Boone** of Texas Instruments was working on quite a similar concept and invented the microcontroller [56]. Boone designed a single integrated circuit chip that could hold nearly all the essential circuits to form a calculator; only the display and the keypad were not incorporated. Surprisingly, this exceptional breakthrough in the field of electronics and communication was rather given a mundane name of **TMS-1802-NC** devise. It had 5000 transistors providing 3000 bits of program memory and 128 bits of access memory. It was possible to program it to perform a range of functions. The image of this first one is present in figure 1.5.
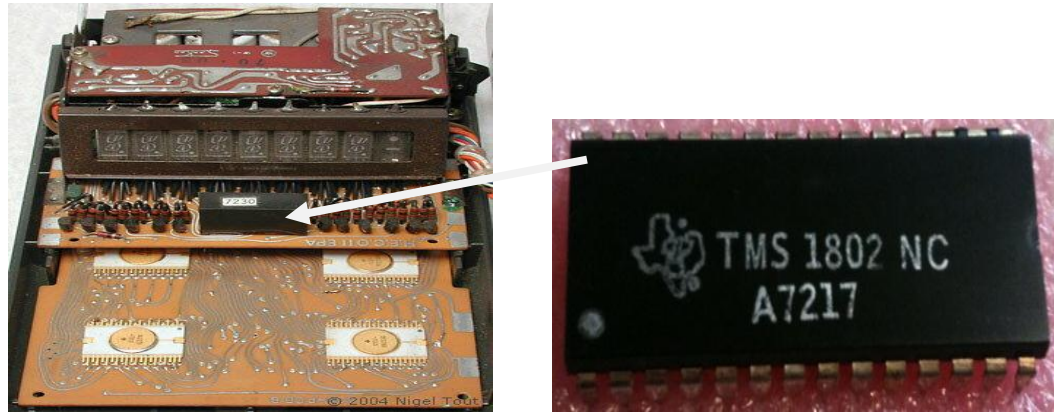
Figure.1.5. (a) First memory calculator built by Intel and (b) the first real and complete microcontroller chip TMS 1802 NC built by Gary Boone.

I-3-1- Definition and structure of microcontrollers

A **microcontroller** is a small computer on a single integrated circuit. In modern terminology, it is similar to, but less sophisticated than, a system on a chip. This system on chip may include a microcontroller as one of its components. A microcontroller contains one or more processor cores along with memory and programmable input/output peripherals. Program memory in the form of ferroelectric RAM or ROM is also often included on chip, as well as a small amount of RAM. Microcontrollers are designed for embedded applications, in contrast to the microprocessors used in personal computers or other general purpose applications consisting of various discrete chips. As we can present, the basic architecture inside of the microcontroller can be simply resume in figure 1.6 as in Ref. [57-59].
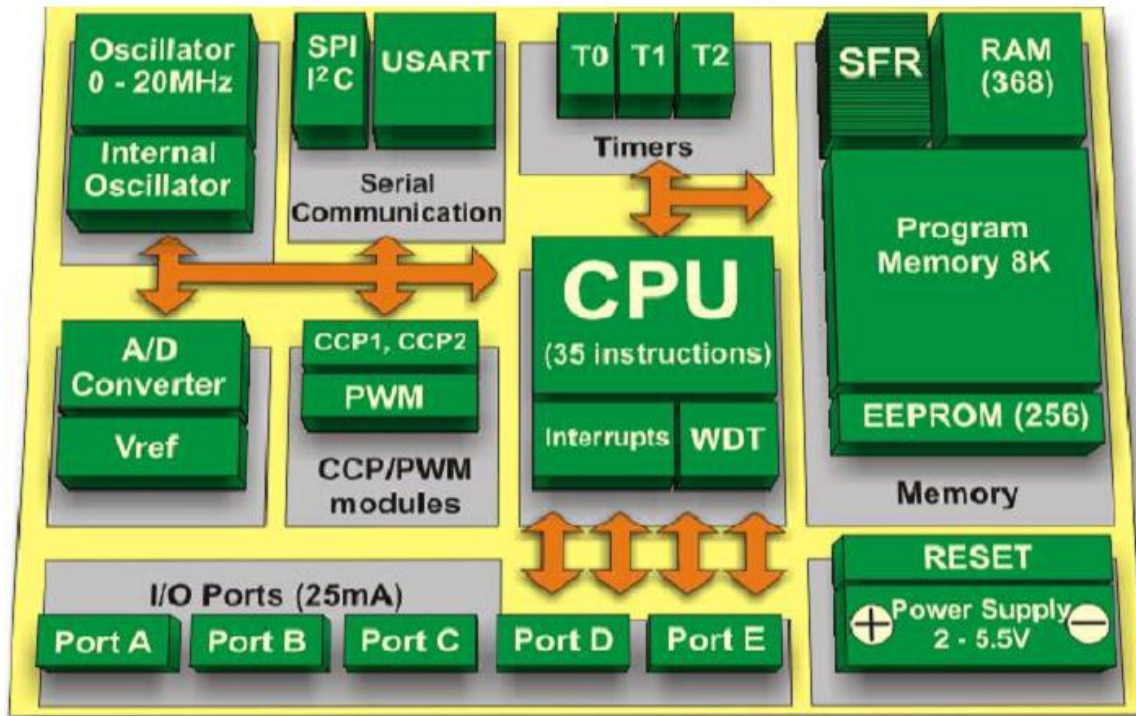
Figure 1.6: Basic architecture inside of the microcontroller (PIC's family).

According to the observations, microcontroller contains eight principle blocs: memory (program memory, EEPROM, SFR), input/output I/O (ports from A to C are the output, D and E, are the input), modulations (CCP1, CCP2 and PMW), serial communication (I²C and USART) and the timer (T0, T1, T2), instructions (CPU, interrupts WDT), converter (A/D), oscillator (QUARTZ) to cadence the executions and RESET (Power Supply). All these blocs work in interaction to produce the digital or analogical results. One also observes that from these different parts cited, it can be simple to conclude that microcontroller contains all the main parts of the computer.

Outside the microcontroller, figure 1.7 presents the names of each pin. Table 1.1 completes the information concerning the microcontroller by presenting the others parameters especially for the PIC18F4550. With the development of embedded technologies, microcontrollers appear today as interesting devices that can help in the mitigation of the limits of the analog electronic circuits [21, 25, 27]. The choice of PIC18F4550 is due to the fact that it is cheap and simple, requires low power (some nanoWatt), presents a large number of utilities ports (three serial ports up to 10 Mbits/s), large amount of RAM memory for buffering and Enhanced Flash program memory and is appropriate for embedded control and monitoring applications that

require periodic connection with a (legacy free) personal computer via USB for data upload, download and firmware updates.

40-Pin PDIP
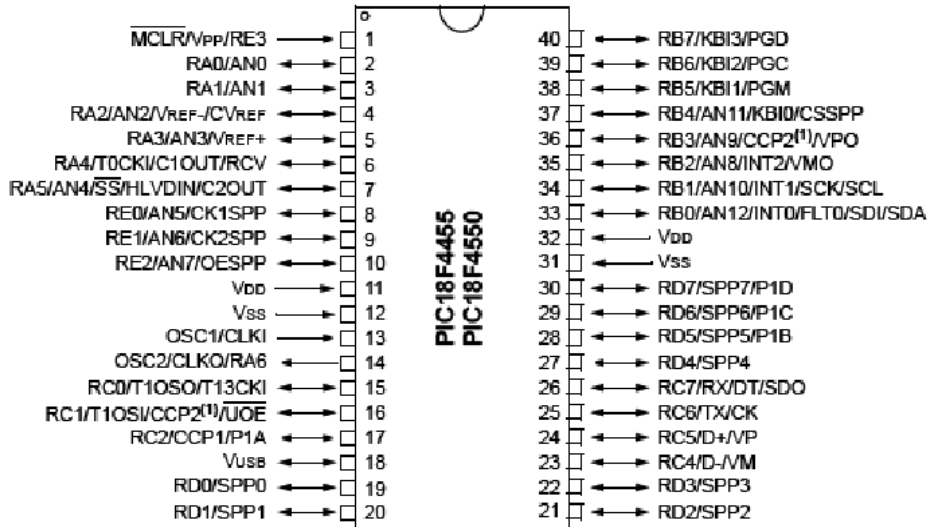
Figure1.7: Pic 18F4550 and it architecture pin's names.

In figure 1.7, we notice that: RA, RB, RC, RD and RE' ports are for the output information, OSCs (oscillation clock) are using to cadenced the pic, MCLR (Microcontroller Clear and Reset) is using to reset the pic, Vss and V_{DD} are voltage polarization.

We can summarize the characteristics of that Pic on table1.1 presents:

PARTS OF MICROCONTROLLER	PARAMETRICS
Program Memory Type	Flash
Program Memory Size (kB)	32
CPU Speed (Mbit/s)	12,16,80
RAM (Bytes)	2,048
Data EEPROM/ (bytes)	256
Digital Communication Peripherals	UART, I^2C
Timers	1 x 8-bit, 3 x 16-bit
ADC Input	13 ch, 10-bit
Number of Comparators	2
Number of USB Modules	1
Temperature Range (°C)	-40 to 85
Pin Count	40

Tab1.1: Presentation of parametric of the Pic 18F4550.

I-3-2- Applications of microcontrollers

Microcontrollers are used in multiple industries and applications, including in the home and enterprise, building automation, manufacturing, robotics, automotive, lighting, smart energy, industrial automation, communications and internet of things deployments. The simplest microcontrollers facilitate the operation of MaEMS found in everyday convenience items, such as ovens, refrigerators, toasters, mobile devices, key fobs, video games, televisions and lawn-watering systems. They are also common in office machines such as photocopiers, scanners, fax machines and printers, as well as smart meters and security systems.

More sophisticated microcontrollers perform critical functions in aircraft, spacecraft, ocean-going vessels, vehicles, medical life-support systems and robots. In medical scenarios, microcontrollers can regulate the operations of an artificial heart, kidney or other organ. They can also be instrumental in the functioning of prosthetic devices [58]. Microcontroller has most applications in life as we can present some of them in the figure1.8.

(a)   (b)

(b)   (d)
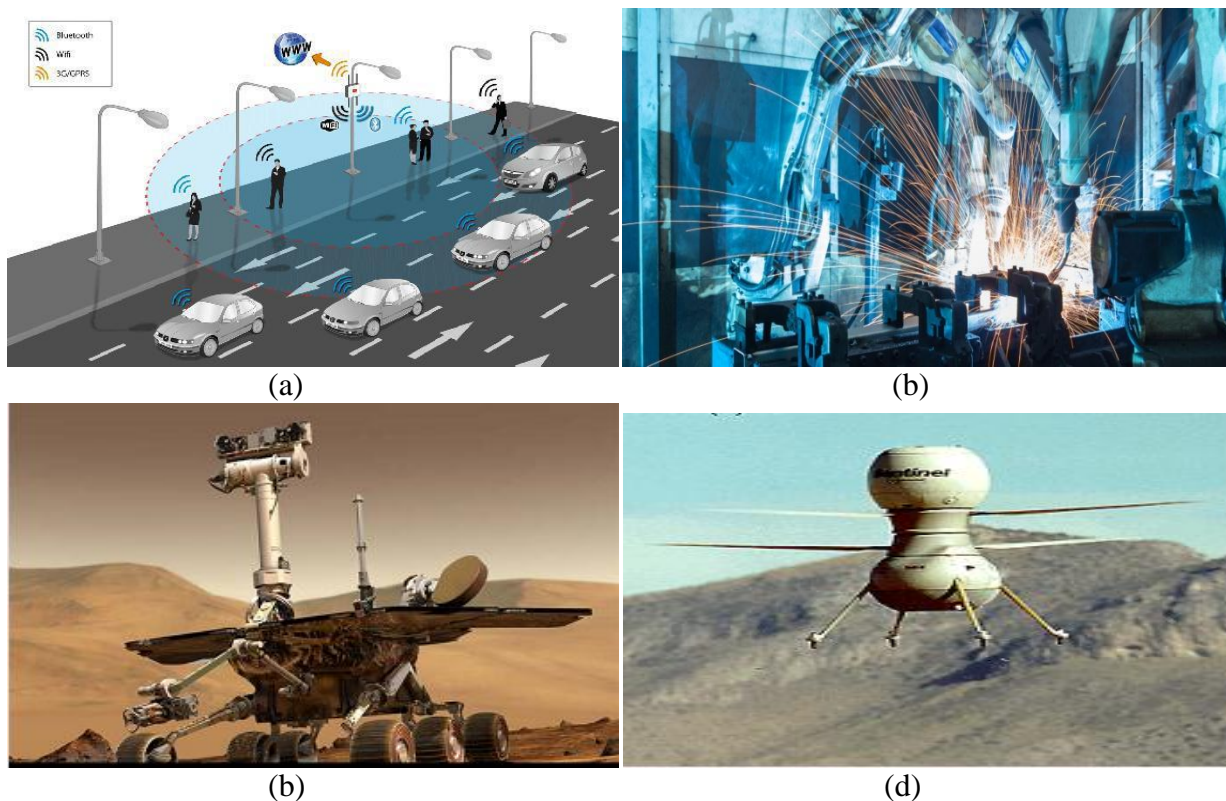
Figure 1.8: Some microcontroller applications. (a)Traffic road, (b) hard and hot work in industry, (c) space exploration and (d) spying's machine.

Today, microcontroller is used in the fundamental researches domain as electronics [25], electro-mechanics and communication [27, 60].

I-3-3- Microcontroller simulation of dynamical systems

Building experimental circuit by using components is one of the difficult roads to achieve fundamental studies in physics. It has been demonstrated recently that microcontroller simulator is more reliable and robust compare to the analog or discrete electronic circuits which have so far been used to study nonlinear dynamical regimes.

Chiu *et al.* implemented for the first time, the chaotic Lorentz oscillator inside the simple PIC microcontroller. In the same ways, many works were followed [25-29]. Based on different research investigations and applications of chaos, microcontrollers are also used in nonlinear dynamics for the main application of chaos phenomenon: the chaos cryptography [27].

In this thesis, theoretical and experimental simulations of dynamical systems (autonomous and non-autonomous Van der Pol oscillator)into a simple microcontroller are performed.

I-4-   Some problems and objectives of the thesis

As presented above, Woafo and Kraenkel investigated different states of synchronization in coupled autonomous and non autonomous Van der Pol oscillators [9]. The stability analysis, numerical simulation and mathematical resolutions were performed to determine the suitable coupling parameters leading to synchronization.

In this thesis, one extends this idea by conducting the experimental investigation on synchronization of two Van der Pol oscillators with polynomial and delay unidirectional couplings.

As indicated in section 1.4.3, microcontrollers are good device to produce complex electrical signals from dynamical systems.

Thus the other objective of this work is to provide a microcontroller implementation of synchronization of two Van der Pol oscillators submitted to disturbances of the pulse-like type. Three cases are taken into consideration: proportional, power order *n* and adaptive coupling.

This leads to the third objective of this thesis which is to power electromechanical systems by signal delivered by microcontrollers.

I-5- Conclusion

In this chapter, we provided some background on Van der Pol oscillator dynamics, synchronization of Van der Pol oscillators, embedded technologies. The problems that we will have to solve in this thesis were also presented. The following chapter will be devoted to the mathematical formalisms, numerical and analog simulations methods used to solve the problems of this thesis.

Chapter II: Theoretical and experimental methods

II-1-   Introduction

This chapter presents the mathematical formalisms, numerical and analog simulations methods, used to solve the problems of this thesis. Section II-2 deals with the mathematical formalisms and numerical methods used to solve the ordinary equations. In section II-3, we present the analog simulation method for dynamical systems, the hardware and software used. In Section II-4, analog construction of differential equation, tools and techniques are presented. Following in section II-5 presents the microcontroller simulation method for differential equations and section II-6 concludes the chapter.

II-2- Mathematical formalisms

In this section II, we present the delayed coupled Van der Pol equations and the approaches to solve these equations. One needs some appropriate mathematical formalism and numerical methods which, are presented here. Depending on the coupling strength, the objective in this subsection is to identify various dynamical states which appear in the master and slave oscillators.

II-2-1- Stability of the synchronization process

In the literature, several different tools to investigate the stability of the synchronization dynamics are proposed, such as the one developed by Butcher and Sinha [61]. But we prefer the Floquet theory [62] which is more indicated to find the stability boundaries. The Van der Pol oscillator is sensitive to initial conditions. When two such oscillators x and u with the same parameters are set into motion with different initial conditions, they evolve in the same limit cycle, but with different phases ψ_1 and ψ_2. The phase lock so that $\psi_2 - \psi_1 = 0$, the good strategy is to use the conventional feedback scheme in the following manner:

$$\begin{cases} \ddot{x} + \mu\left(x^2 - 1\right)\dot{x} + \omega_0^2 x = 0, \\ \ddot{u} + \mu\left(u^2 - 1\right) + \omega_0^2 u = k(u - x_\tau)H(t - T_0). \end{cases} \tag{2.1}$$

x is the master function and u the slave one, k is the feedback strength as presented in [63]. The delay τ here means the time spends by the master signal to come and forced the slave one.

To find the stability or synchronization limits, one introduces the variable z defines as

$$z = u - x_\tau.$$
(2.2)

When introducing z in Eq. (2.1) and considering only linear terms, one obtains the following equation:

$$\ddot{z} = l\left(\dot{z}, \dot{x}_\tau, z, x_\tau, k\right).$$
(2.3)

where l is a function. Assuming small parameter of the functions of the nonlinearity, the delayed dynamics function can be described by:

$$x_\tau = A\cos(\omega, \beta, \tau).$$
(2.4)

where the amplitude A and the frequency ω depend on the nonlinear parameter and β, the parameter depending on the different of phase and time t. Inserting in equation (2.3), one obtains the variational equation (2.5).

$$\ddot{z} = j\left(z, \dot{z}, F(\beta,\tau), G(\beta,\tau)\right).$$
(2.5)

where j is a function, $F(\beta,\tau)$ and $G(\beta,\tau)$ are the functions depending on the parameter of the system, delay τ and β.

To discuss further the stability process, one rewrites Eq. (2.5) in a standard form. For this purpose, one uses the transformation

$$z = W \exp\left(-\int_0^\beta \left(\lambda + \frac{1}{2}F(\beta',\tau)\right)d\beta'\right).$$
(2.7)

Introduce Eq. (2.7) in Eq. (2.5) one obtains the hill equation given by Equation (2.8) below

$$\ddot{W} + p\left(k, \cos(\beta), \sin(\beta), \cos(\tau), \sin(\tau)\right)W = 0.$$
(2.8)

where p is a function depending on β, k and τ.

II-2-2- Whittaker formalism

To solve Eq.(2.8), one uses the Whittaker formalism [9]by writing

$$W = \exp(\rho\beta)\sin(n\beta - \sigma) \quad \text{with } n=1,2.$$
(2.9)

ρ here means the characteristic exponent and σ one simple parameter. Substituting W into the Hill polynomial as in Eq. (2.8), one finds that ρ is the solution of the equations (2.10).

$$\begin{pmatrix} a_{11}(\tau) & a_{12}(\tau) \\ a_{21}(\tau) & a_{22}(\tau) \end{pmatrix} \begin{pmatrix} \cos(\sigma) \\ \sin(\sigma) \end{pmatrix} = \begin{pmatrix} 0 \\ 0 \end{pmatrix}, \tag{2.10}$$

where $a_{ij}(\tau) = 2\sum_{l=1}^{2} a_{ls}(\tau)$ or $2\sum_{l=1}^{2} a_{lc}(\tau)$ are the parameters of the Hill functions. Equations (2.10) have solutions different to zero if and only if

$$\Delta = a_{11}(\tau)a_{22}(\tau) - a_{21}(\tau)a_{12}(\tau) = 0. \tag{2. 11}$$

Solving equation (2. 11) allows us to better determine the analytical expression of the strength parameter k leading to synchronization.

II-2-3- Development of the method

When introducing z in Eq. (2.1) and considering only linear terms, one obtains the following equation:

$$\ddot{z} - \mu(1 - x_\tau^2)\dot{z} + (2\mu x_\tau \dot{x}_\tau + 1 - k)z = 0. \tag{2.12}$$

Assuming small μ, the master dynamics can be described by:

$$x_\tau = A\cos(\omega t - \psi_1 - \omega\tau). \tag{2.13}$$

where the amplitude A and the frequency ω depend on μ. If we let $\beta = \omega t - \psi_1$, inserting in the equation (2.12), one obtains the variational equation (2.14).

$$\ddot{z} + (2\lambda + F(\beta))\dot{z} + G(\beta)z = 0. \tag{2.14}$$

where the functions have the expression given below in Eq.(2.15)

$$\lambda = \frac{\mu}{2\omega}\left(\frac{A^2}{2} - 1\right)$$

$$F(\beta) = \frac{\mu A^2}{2\omega}\cos(2\omega\tau)\cos(2\beta) + \frac{\mu A^2}{2\omega}\sin(2\omega\tau)\sin(2\beta) = F_1(\tau)\cos(2\beta) + F_2(\tau)\sin(2\beta)$$

$$F_1(\tau) = \frac{\mu A^2}{2\omega}\cos(2\omega\tau) \quad and \quad F_2(\tau) = \frac{\mu A^2}{2\omega}\sin(2\omega\tau) \tag{2.15}$$

$$G(\beta) = \frac{1-k}{\omega^2} - \frac{\mu A^2}{\omega}\cos(2\omega\tau)\sin(2\beta) + \frac{\mu A^2}{\omega}\sin(2\omega\tau)\cos(2\beta) = G_1 - G_2(\tau)\sin(2\beta) + G_3(\tau)\cos(2\beta)$$

$$G_1 = \frac{1-k}{\omega^2}; \quad G_2(\tau) = \frac{\mu A^2}{\omega}\cos(2\omega\tau) \quad and \quad G_3(\tau) = \frac{\mu A^2}{\omega}\sin(2\omega\tau).$$

From the expression of G_1, we find that if $k > 1$, z will grow indefinitely leading the slave to continuously drift away from its original limit cycle. In this case, the feedback coupling is dangerous since it continuously adds energy to the slave system. This boundary, obtained here from the simple analytical consideration, has been observed by Leung [64-65].

To discuss further the stability process, one rewrites Eq. (2.14) in a standard form. For this purpose, we use the transformation

$$z = W \exp\left(-\int_0^\beta \left(\lambda + \frac{1}{2} F(\beta') \right) d\beta' \right). \tag{2.16}$$

Introduce Eq. (2.16) in Eq. (2.14) one obtains the Hill equation given by Equation (2.17) as

$$\ddot{W} + \left(a_0 + 2a_{1s}\sin(2\beta) + 2a_{1c}\cos(2\beta) + 2a_{2c}\cos(4\beta) + 2a_{2s}\sin(4\beta) \right) W = 0. \tag{2.17}$$

From Eq. (2.17), the parameters are

$$a_0 = \frac{1}{\omega^2}\left[1 - K - \frac{\mu^2}{4}\left(\frac{A^2}{2} - 1 \right)^2 - \frac{\mu^2 A^4}{32} \right];$$

$$a_{1s}(\tau) = -\frac{\mu A^2}{2\omega}\left[\cos(2\omega\tau) + \sin(2\omega\tau) \right];$$

$$a_{1c}(\tau) = -\frac{\mu^2 A^2}{16\omega^2}\left(A^2 - 2 \right)\cos(2\omega\tau) - \frac{\mu^2 A^2}{2\omega}\sin(2\omega\tau); \tag{2.18}$$

$$a_{2c}(\tau) = -\frac{\mu^2 A^4}{64\omega^2}\cos(4\omega\tau);$$

$$a_{2s}(\tau) = -\frac{\mu^2 A^4}{64\omega^2}\sin(4\omega\tau).$$

For analyse deeply this stability process, let consider the adapted method which is the Whittaker formalism.

> ➤ **Whittaker formalism**

Solves Hill equation became to discuss the strength parameters k. For achieved the resolution of Eq. (2.17), one use the Whittaker formalism [9] which consists to discuss about the stability of this strength parameters. To investigate this procedure, let considered W given below

$$W = \exp(\rho\beta)\sin(n\beta - \sigma) \quad \text{with } n=1, 2. \tag{2.19}$$

ρ here means the characteristic exponent of the stability and σ one simple parameter. Substitute W in the Hill equation Eq. (2.17), one found that ρ is the solution of the system equations (2.20) given below

$$\begin{pmatrix} a_{ns}(\tau)+2\rho n & \rho^2-n^2+a_0+a_{nc}(\tau) \\ \rho^2-n^2+a_0-a_{nc}(\tau) & a_{ns}(\tau)-2\rho n \end{pmatrix}\begin{pmatrix} \cos(\sigma) \\ \sin(\sigma) \end{pmatrix}=\begin{pmatrix} 0 \\ 0 \end{pmatrix}; \tag{2.20}$$

where $a_{ns}(\tau)=2\sum_{i=1}^{2}a_{is}(\tau)$ and $a_{nc}(\tau)=2\sum_{i=1}^{2}a_{ic}(\tau)$ are the parameters of the Hill function. The system of equations (2.20) has solution different to zero if and only if

$$\left(a_{ns}(\tau)+2\rho n\right)\left(a_{ns}(\tau)-2\rho n\right)-\left(\rho^2-n^2+a_0-a_{nc}(\tau)\right)\left(\rho^2-n^2+a_0+a_{nc}(\tau)\right)=0. \tag{2.21}$$

According to Eq. (2.21), one obtains:

$$\rho^2=-n^2-a_0\pm\sqrt{4n^2a_0+a_n^2(\tau)} \text{ with } a_n^2(\tau)=a_{ns}^2(\tau)+a_{nc}^2(\tau). \tag{2.22}$$

The synchronization process is stable when z in Eq. (2.14) goes to zero with increasing time. In that case, the real part of $-\lambda\pm\rho$ should be negatives. According to this consideration, the stability condition can be taken as

$$\lambda^2\geq\rho^2. \tag{2.23}$$

Consequently, the synchronization process is stable under the condition concerning the Hill function:

$$H_n=\left(a_0-n^2\right)^2+2\left(a_0-n^2\right)\lambda^2+\lambda^4>a_n^2(\tau). \tag{2.24}$$

This expression can be transform into the new expression allow us to obtain analytically the expression of the strength parameter depending of the delay. That is given by (2.25) below

$$-\frac{k(\tau)^2}{\omega^4}+2\left(n^2-a_{01}-\lambda^2\right)\frac{k(\tau)}{\omega^2}+\left[a_{01}^2-2n^2a_{01}+n^4+2a_{01}\lambda^2+2n^2\lambda^2+\lambda^4-a_n^2(\tau)\right]>0$$

$$(2.25)$$

where $a_{01}=\dfrac{1}{\omega^2}\left[1-\dfrac{\mu^2}{4}\left(\dfrac{A^2}{2}-1\right)^2-\dfrac{\mu^2A^4}{32}\right]$ and under the stability condition (2.26)

$$a_n^2(\tau) < 4n^2\lambda^2 \tag{2.26}$$

This last condition is satisfied only for $n = 1$.

II-3-Numerical methods

II-3-1- Fourth-order Runge-Kutta method for ODEs

Runge-Kutta (RK) methods is one of the important numerical methods that we have used to solve the ODEs. It follows the scheme given below. Let consider the following ordinary differential equation:

$$\frac{dX(t)}{dt} = f(X(t), t) \text{ with } X(t_0) = X_0; \tag{2.27}$$

where $f = (f_1, f_2, \ldots, f_n)$ is a vectorial function with the unknown vectorial variable $X(t) = (x_1(t), x_2(t), \ldots, x_n(t))$.

The RK4 scheme for this problem is given by [66-67]:

$$x_{i+1} \leftarrow x_i + \frac{1}{6}\left(L_1 + 2\left(L_2 + \bar{L}_3\right) + L_4\right),$$
$$t \leftarrow t + \Delta t, \tag{2.28}$$

where

$$
\begin{aligned}
L_1 &\leftarrow \Delta t \cdot f(x_i, t), \\
L_2 &\leftarrow \Delta t \cdot f(x_i + L_1/2, t + \Delta t/2), \\
L_3 &\leftarrow \Delta t \cdot f(x_i + L_2/2, t + \Delta t/2), \\
L_4 &\leftarrow \Delta t \cdot f(x_i + L_3, t + \Delta t),
\end{aligned}
\tag{2.29}
$$

and i runs for time incrementation related to x_i. L_1, L_2, L_3 and L_4 are intermediate coefficients and Δt is the time step.

II-3-2- Second-order delayed Runge-Kutta method for DDEs

In the case of DDEs, the dynamics at each t depends on the value of the vector X at the same instant t and at $t-\tau$, with $\tau > 0$ is the delayed parameter [67-68]. If one introduces the delayed variable $X(t-\tau)$, the ODEs becomes

$$\frac{dX(t)}{dt} = f\left(X(t), X(t-\tau), t\right) \text{ for } t \in [0, \tau].$$
(2.30)

where, $f = (f_1, f_2, ..., f_n)$ is a vectorial functions with the unknown vectorial variables $X(t) = (x_1(t), x_2(t), ..., x_n(t))$ and $X(t-\tau) = (x_1(t-\tau), x_2(t-\tau), ..., x_n(t-\tau))$ with the initial condition $x(0) = y(t = 0)$, when $t \in [-T, 0[$, T is the temporal amplitude of delay. The initial condition is a constant function in the finite interval. Let consider $N_T = \dfrac{T}{\Delta t}$, $t = i\Delta t$ where i in an integer and Δt is the time step. The solution of this equation is given by the RK2 scheme for ODEs [69] as follows

$$x_{i+1} = x_i + \frac{1}{2}(L_1 + L_2),$$
$$t = t + \Delta t,$$
(2.31)

where

$$L_1 = \Delta t \cdot f\left(x_i, x_{\tau-N_T}, i\Delta t\right),$$
$$L_2 = \Delta t \cdot f\left(x_i + L_1, x_{\tau-N_T+1}, (i+0.5)\times\Delta t\right),$$
(2.32)

where i runs for time incrementation and the variables related to x_i L_1, L_2 are intermediate coefficients.

II-3-3- Numerical criteria for synchronization

In the numerical procedure, we consider that synchronization is achieved, when the deviation z obeys the following synchronization condition

$$|z| = |x - u| < \varepsilon, \ \forall \ t \geq T_{syn},$$
(2.33)

where x is the master and u the slave oscillators, ε the synchronization process or tolerance, T_{syn} the synchronization time instant at which the two trajectories are close enough to be considered as synchronized.

II-4- Analog construction of DEs

II-4-1- Electrical components

To design electronically the mathematical operations (addition, substraction, derivatives, intergrals and multications), one needs to combine the basic electrical components such as resistors, capacitors and inductances with operational amplifiers and analog multipliers.

o **Operational amplifier**

The Operational Amplifier (Op-Amp) is an integrated circuit that which amplifies an input through a very high gain. The Op-Amp contains several transistors. An operational amplifier has two input terminals used for polarization. It has also two inputs which are the non-inverting and inverting inputs. Figure 2.1a presents an example of operational amplifier. Finally it has one terminal output used to obtain the output signal (see figure 2.1b).
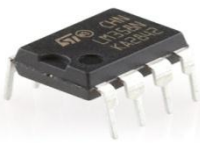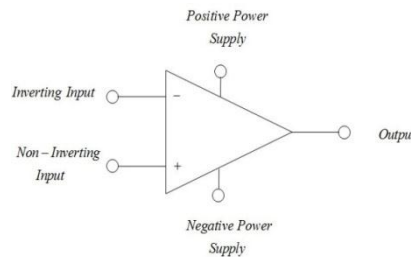
(a)   (b)

Figure 2.1: (a) Operational amplifier component and (b) electrical equivalent of the operational amplifier.

o **Analog multiplier**

An analog multiplier produces an output signal which is the product of two input voltages. Figure 2.2 presents in (a) an example of analog multiplier and in (b) its equivalent electronic circuit [70]. Such circuits can be used to implement polynomial nonlinear functions. In the market, one can find different types of analog multipliers. The most used is the AD633 family

analog device. The multiplication of the voltage differences $(X_1 - X_2)$ and $(Y_1 - Y_2)$ over 10 Volts is added to the offset voltage Z and the sum is obtained at the output terminal.

(a)   (b)

Figure 2.2: (a) Example of analog multiplier AD633JN and (b) electrical equivalent of the analog miltiplier.

II-4-2- Principle of construction of differential terms of a differential equation

This section presents the basic analog operations used to design the electronic circuits for differential equations. Analog simulation principle is universal and its elementary operations are direct consequences of physics laws [71]. The basic operations are: summation, multiplication integration and derivation which are presented in figure 2.3

(a) Summation   (b) Inversion
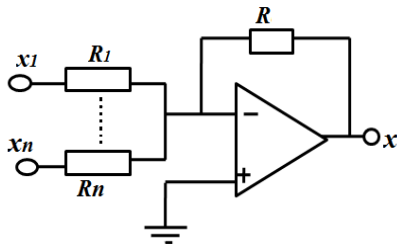
$$x = a_1 x_1 + a_2 x_2 + ... + a_n x_n \text{ with } a_1 = \frac{R}{R_1}, \ a_2 = \frac{R}{R_2}, ..., a_n = \frac{R}{R_n}$$
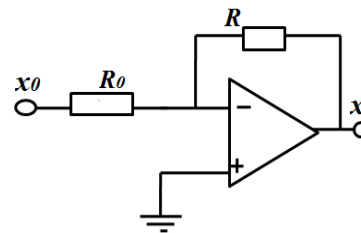
$$x = a x_0 \text{ with } a = -\frac{R}{R_0}$$

(c) Derivation   (d) Integrator
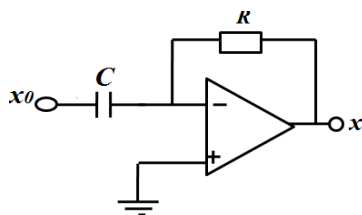
$$x = a \frac{dx_0}{dt} \text{ with } a = -RC$$
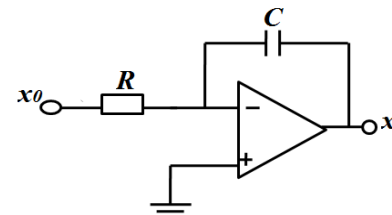
$$x = a \int x_0 dt \text{ with } a = -\frac{1}{RC}$$

Figure.2.3: Basic linear operations with Op-Amp.(a) summation, (b) inversion, (c) derivation and (d) integration

For the multiplication, according to the bloc diagram showing the electrical equivalent of the multiplier in Figure 2.4(b), the output signal W is given as

$$W = \frac{(X_1 - X_2)(Y_1 - Y_2)}{10} + Z. \qquad (2.34)$$

II-4-3-   Analog construction of the coupling

We use also the Op-Amp and linear components (resistors) to build the coupling function. This circuit is called differentiator. Figure 2.4 presents the bloc of coupling function.

$$x = \frac{R_0}{R}(x_2 - x_1)$$
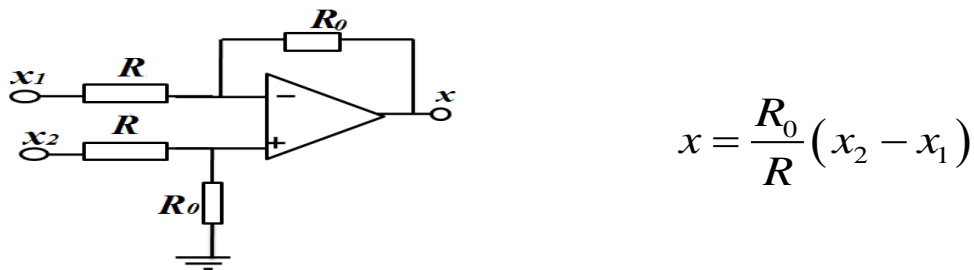
Figure 2.4: Coupling function.

In this thesis, we build the coupling function of power n by using the multipliers and the bloc of figure 2.4. For that propose, we consider that all the resistors are identical $R = R_0$. Figure 2.5 presents the situation for each power degree.

(a) $x = (x_2 - x_1)$ (b) $x = (x_2 - x_1)^2$ (c) $x = (x_2 - x_1)^3$
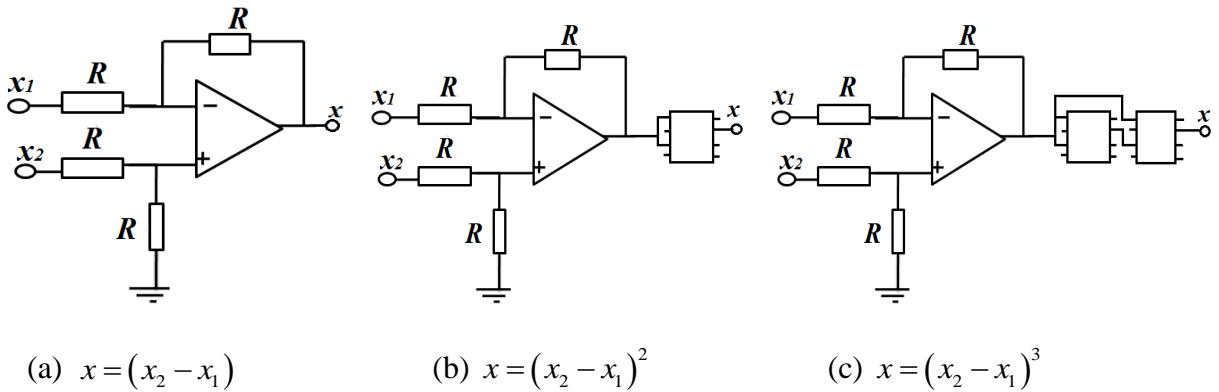
Figure. 2.5: Analog equivalent of coupling of power n.

II-5- Microcontroller simulation of DEs.

II-5-1- Principle

To program DEs in microcontroller, one needs to follow these different steps.

o **Discrete form of equation**

Many methods exist to discretize the DEs. In the literature, we can have Euler, Runge-Kutta of order 2 and 4, Runge-Kutta-Simpson, Adams-Bashforth methods and so on. The discrete equations can be implemented in a microcontroller program. In this thesis, we will use most of the time the Euler scheme.

o **Program languages inside the microcontroller**

To build a result coming from that component, one should know different languages of programming as C, C^{++}, Assembler, Java Script, C for arduino and so on. The execution should be done by having the computer with software (Ccs blog, mikroC for PIC, Arduino...) installed inside. Using the C language and by the mickroC for PIC, one implements the discrete equations inside the microcontroller.

o **Insertion inside the microcontroller**

In electronic simulation domain, much of the software is used as Multisim, Pspice, Proteus and so on. Proteus is the software that we used to simulate the signal coming from differentials equation after programming in microcontroller software. One of the most advantages of Proteus is it includes microcontroller family of the PIC simulation, as well as integrated import and export features to the printed circuit board. After simulation in mikroC for PIC or Arduino and Proteus, one uses the setup presented in Figure 2.6 to insert the signal inside the microcontroller.

Figure 2.6: Image of the implementation setup.

o **Analog signal outside the microcontroller**

. To obtain analog signal coming from the microcontroller, one has an active converter DAC0808 which needs external energy and a passive one built with resistors(R-2R) which does not need external energy. The one we use is the passive converter. The ports B and D of the microcontroller were coupled to a R-2R ladder resistors network, acting as a DAC (digital to analogical converter) (see figure 2.7).

The microcontroller and the R-2R DAC were selected because they are cheap and very simple to configure. It works by the principle of superposition where switching on binary inputs adds more voltage at the output. Using a ladder network is a common way of creating an 8 bit DAC as each control bit contributes to a binary weighted output voltage. It presents a low experimental error of 4.16 %. The outputs of the DAC ports were taken from the resistors labelled as R7 and R16, and they correspond to outputs respectively [25]. After the signal passing cross the network of resistors then connected the cable to the oscilloscope, we obtain the analogical signal.

II-5-2- Structure of operational bloc

Figure 2.8 shows the operational bloc. To filter the signal out of the DAC, one uses the capacitors C_1 and C_2 to obtain clear and good signals coming from the microcontroller and viewed in the oscilloscope [72].
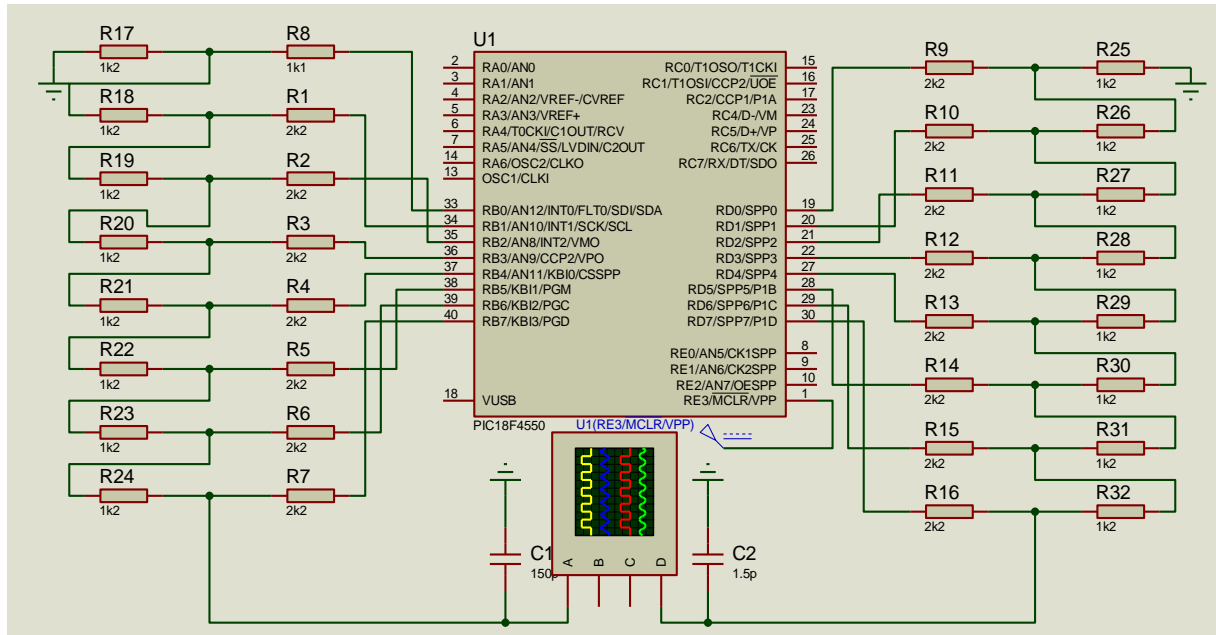
Figure 2.7: Electronic circuit used to implement in a microcontroller the controlled and synchronized Van der pol oscillators.

II-6-   Conclusion

This chapter has been devoted to the presentation of the different methods used in the thesis. Firstly, we have presented the mathematical formalisms used to find synchronization condition. Secondly, the numerical methods have been presented. Thirdly, we have provided the basic principles of analog simulations techniques. Finally the new method using microcontrollers to simulate differential equations has been presented. The results obtained in the course of our PhD research works are presented in the next chapter.

Chapter III: Results and discussions

III-1- Introduction

This chapter presents the results obtained in the thesis. In the first section, the analogical simulation results of the delayed coupled Van der Pol oscillator are presented. The second one is devoted to synchronization and control simulation using microcontroller and the third one is on the fabrication of a self-sustained nonlinear signal generator.

III-2- Synchronization of Van der Pol oscillatiors: analog simulation results

The aim of this section is to present the mathematical models and build the corresponding electrical circuits. These electrical models will be used to find the experimental synchronization strength parameter in different cases as polynomial coupling, delayed coupling both for autonomous and excited Van der Pol oscillators.

III-2-1- Mathematical models

Considering our proposed model taking into account the power on the control function and the excitation form, the coupled Van der Pol oscillators appear in equation (3.1)

$$
\begin{aligned}
&\ddot{x} - \mu(1-x^2)\dot{x} + x = E_m \cos(\Omega t), \\
&\ddot{u} - \mu(1-u^2)\dot{u} + u = E_m \cos(\Omega t) + k(u-x)^n H(t-T_0),
\end{aligned}
\tag{3.1}
$$

where n is the integer parameter, $n \in \{1,2,3,...\}$ Ω and E_m are respectively the frequency and amplitude of the excited function.

From this mathematical model, one has built the electrical models presented in the subsection below.

III-2-2 Electronic circuits for experiments

The circuit's diagrams of the oscillators are shown in figure 3.1 for the three values of n. These oscillators were built using the multipliers AD633 JN and operational amplifiers TL-082. The TL-082 was used to minimize the output drift due to offset and bias current. The term

$(u-x)^n$ is built by using operational amplifiers and multipliers. The different circuits on figure 3.1 are those used in experiment.
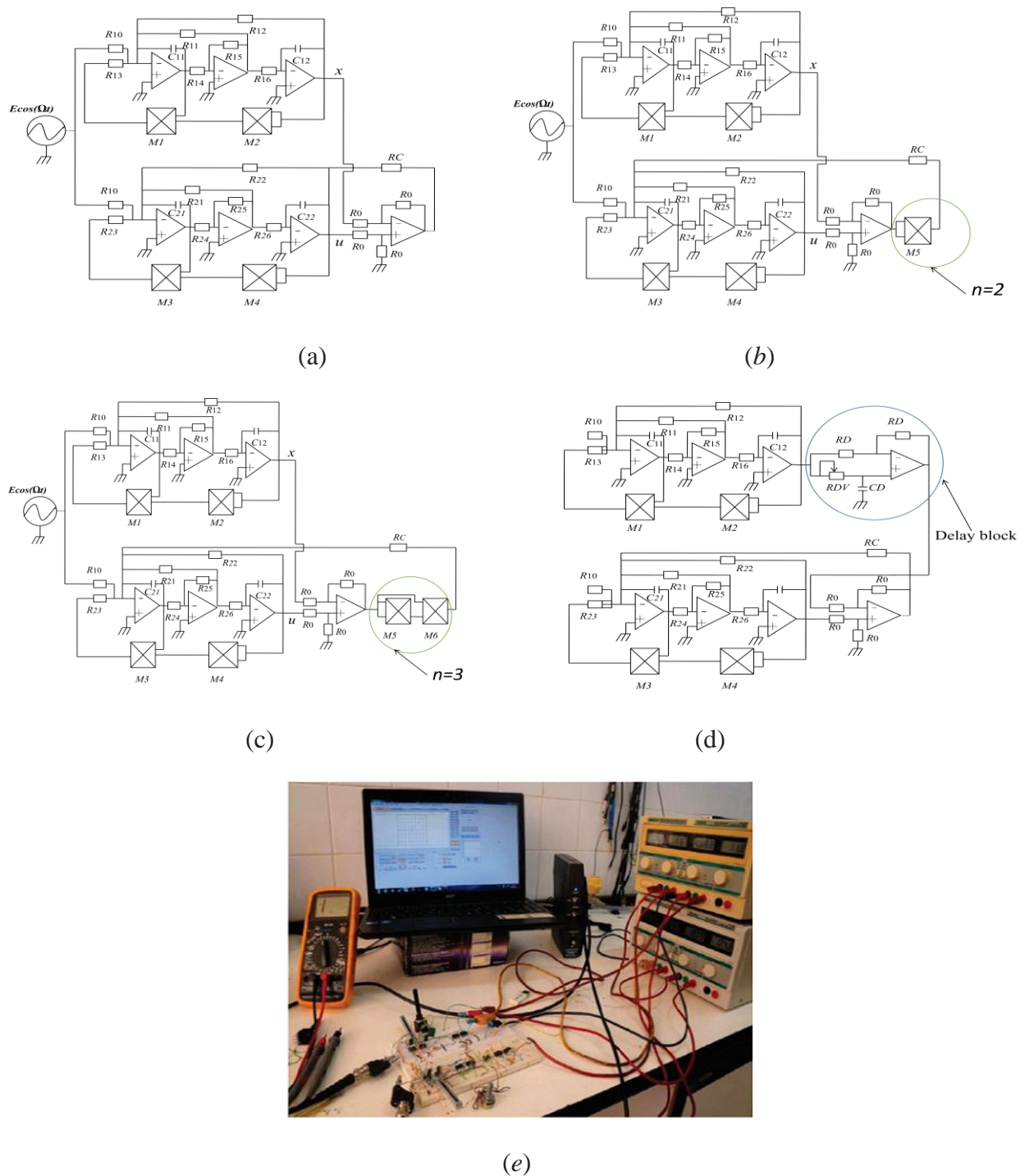

(a)

(b)

(c)

(d)

(e)

Figure 3.1 Electronic schemes of the oscillators: (*a*) linear coupling for n = 1, (*b*) square nonlinear coupling for n = 2, (*c*) cubic nonlinear coupling for n = 3 and (*d*) delayed coupling circuit and (*e*) experimental circuit in operation in the laboratory.

Applying the Kirchhoff's law in each circuit and use: $s=\omega_{01}t=\omega_{02}t$, where s is the dimensionless parameter, ω_{01} and ω_{02} arethe equal natural frequencies; one globally obtains the differential equations (3.3).

$$\frac{d^2x}{ds^2}=\frac{1}{R_{14}C_{11}\omega_{01}}(1-x^2)\frac{dx}{ds}-\frac{R_{15}}{R_{12}R_{14}R_{16}C_{11}C_{12}\omega_{01}^2}x+\frac{R_{12}}{R_{10}}E\cos(\Omega t),$$

$$\frac{d^2u}{ds^2}=\frac{1}{R_{24}C_{21}\omega_{02}}(1-u^2)\frac{du}{ds}-\frac{R_{25}}{R_{22}R_{24}R_{26}C_{21}C_{22}\omega_{02}^2}u+\frac{R_{22}}{R_{10}}E\cos(\Omega t)+\frac{R_{22}}{R_C}(u-x)^n,\ n=\{1,\ 2\ and\ 3\},$$

(3.3)

Then, we set the parameters:

$$\mu_1=\frac{1}{R_{14}C_{11}\omega_{01}};\ \mu_2=\frac{1}{R_{24}C_{21}\omega_{02}};\ \omega_{01}^2=\frac{R_{15}}{R_{12}R_{14}R_{16}C_{11}C_{12}};\ \omega_{02}^2=\frac{R_{25}}{R_{22}R_{24}R_{26}C_{21}C_{22}}$$

$$k=\frac{R_{22}}{R_C},\ E_{m1}=\frac{R_{12}}{R_{10}}E\ and\ E_{m2}=\frac{R_{22}}{R_{10}}E.$$

(3.4)

Since, we assume identical oscillators, we can set

$$R_{14}=100R_{13}\ and\ R_{24}=100R_{23}.$$

(3.5)

and $\mu_1=\mu_2=\mu;\ E_{m1}=E_{m2}=E_m\ and\ \omega_{01}=\omega_{02}.$

(3.6)

The relation between the damping coefficient d and the resistance R_{16} and R_{26} is given by:

$$\mu=3.1\times10^{-3}\sqrt{R_{16}}=3.1\times10^{-3}\sqrt{R_{26}}.$$

(3.7)

One can thus vary d by adjusting the value of R_{16} or R_{26} using a potentiometer. The experimental values of the resistances and capacitors are given in the Table 3.1.

Résistors (kΩ) Capacitors (nF)	Oscillators 1 & 2
$R_{13}=R_{23}$	0.1
$R_{11}=R_{21}$	10.0
$R_{12}=R_{22}$	1.0
$R_{15}=R_{25}$	10.0
R_{10}	0.1
$R_{14}=R_{24}$	10.0
R_0	180.0
R_C	0 – 22 (potentiometer)
$C_{11}=C_{21}$	12.0
$C_{12}=C_{22}$	12.0

Table 3.1 Experimental values of the resistors and capacitors used.

To better present the result coming from all these electrical circuits, let start by the synchronization intervals in the case of polynomial coupling then study the effect of delay.

III-2-3 Synchronization intervals in the case of polynomial coupling

In this section, two cases will be presented to better study these synchronization intervals. For the first, we will study the case of $E_m=0$ and the second E_m taking different values.

o **Coupling intervals for synchronization in the autonomous case ($E_m=0$).**

Let us start with the case where the autonomous Van der Pol oscillator exhibits sinusoidal oscillation. This is obtained by having small value for the nonlinear damping coefficient μ. Taking $R_{16}=R_{26}=10$ $k\Omega$, one obtains $\mu=0.31$. To detect experimentally the synchronization intervals, we vary Rc using a potentiometer. Table 3.2 summarizes our findings along with the boundaries giving by the numerical simulation.

n	μ	Synchronization boundaries obtained from the numerical simulation of equations (3.1) with Em=0 (k)	Synchronization boundaries obtained from the experiment R_C and (k)
1	0.3	$k \in [0.15;1[$	$R_C \in [0.653, \ 1.15]k\Omega,$ this corresponds to $k \in [0.87;1.53]$
2	0.3	$k \in [0.09;0.18[$	$R_C \in [2.37, \ 9.61]k\Omega$ this corresponds to $k \in [0.104;0.421]$
3	0.3	$k \in [0.06;0.13[$	$R_C \in [0.65; \ 0.74]k\Omega$ this corresponds to $k \in [1.37;1.52]$

Table 3.2 Synchronization intervals obtained experimentally and through numerical simulation for $\mu=0.3$ and different degrees of the coupling polynomials.

From Table 3.2, one finds that the synchronization interval decreases as the nonlinearity in the coupling increases. Otherwise, one observes that the amplitude of the intervals of the experimental results decreases when the values of n increase. Numerically, the intervals of the coupling parameter decrease when n increases particularly at the borders.

Due to experiment artifacts, the boundaries of intervals generated from the experiment are different to those obtained by the numerical simulation. Indeed, the numerical simulation assumes perfectly identical oscillators while in the experiment; it is not possible to have perfect identical oscillators. These explanations also hold for the results presented in the rest of the work.

As indicated above, the synchronization is decided during the numerical simulations by using the condition at Eq (2.33) or using the phase portrait (x, u). In the experiment, the synchronization is decided by plotting the phase portrait in the (x, u) plane. Figure 3.2 presents an example of phase portraits before the coupling and Figure 3.3 when there is no synchronization despite the coupling while Figure 3.4 presents a state of synchronization.

(a)   (b)

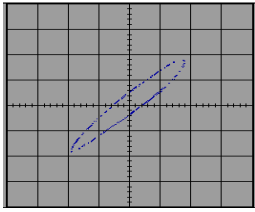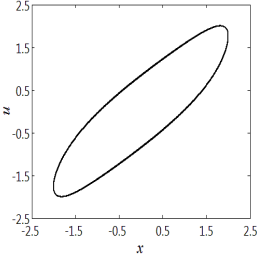Figure 3.2 Phase portrait exhibited by one oscillator before the coupling: (a) Experiment and (b) Numerical.
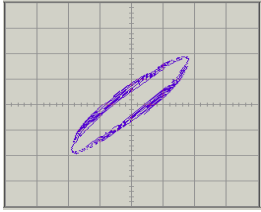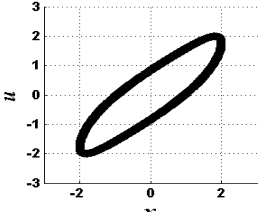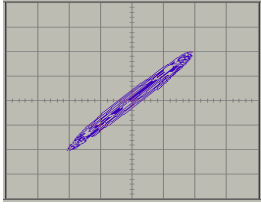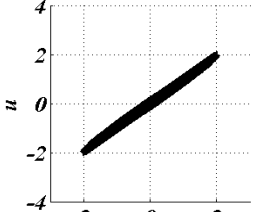
n, k and R_C values	Experimental results	Numerical results
n=1 *R_C=90 kΩ* *Corresponding to k=0.056.*	 (a)	 (b)
n=2 *R_C=34.1 kΩcorresponding to* *k=0.15*	 (c)	 (d)
n=3 *Rc=73 kΩ corresponding to* *k=0.07.*	 (e)	 (f)

Figure 3.3 Phase portraits: (a)-(f) are for the coupled oscillators showing the case of no synchronization for different values of parameters n, k and R_C in the case of μ=0.3.

After coupling the oscillators, one finds the synchronized situation and Figure 3.4 displays this case with different values of *n*, *Rc* and their corresponding values *k*.
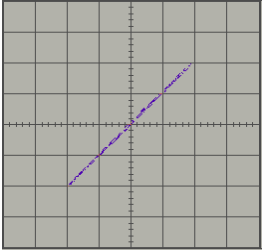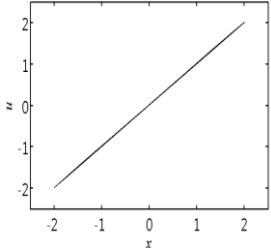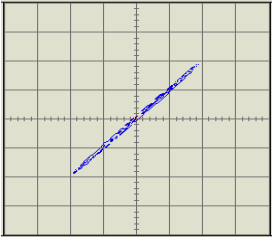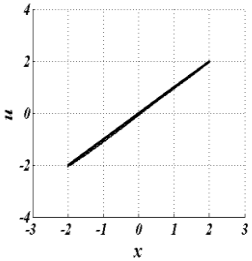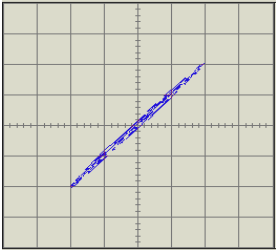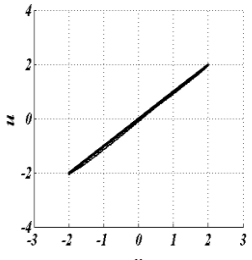
n, k and R_C values	Experimental results	Numerical results
n=1 R_C=73 kΩ corresponding to k=0.07.	 (a)	 (b)
n=2 R_C=51 kΩ corresponding to k=0.1.	 (c)	 (d)
n=3 R_C=63.75 kΩ corresponding to k=0.08.	 (e)	 (f)

Figure 3.4 Phase plans (a)-(f) are for the coupled oscillators showing the case of synchronization for different values of *n* in the case of μ=0.3.

From both these tables, one observes some good agreements between the numerical and experimental results.

Now let us consider the state where the autonomous Van der Pol delivers relaxation oscillations. They are obtained for large values of μ. We have considered $\mu=5$ corresponding to

$$\mu_1 = 3.162 \times 10^{-3}\sqrt{R_{16}} \text{ et } \mu_2 = 3.162 \times 10^{-3}\sqrt{R_{26}} \qquad (3.8)$$

To obtain that value of μ, one takes $R_{16}=R_{26}=25M\Omega$. The synchronization intervals are displayed in Table 3.3.

n	μ	Synchronization boundaries obtained from the numerical simulation of equations (3.1) with $E_m=0$ (k)	Synchronizations boundaries obtained from the experiment R_C and (k)
1	5	$k \in \,]0.01;\ 1[$	$R_C \in [0.653,\ 1.15]\ k\Omega,$ this corresponds to $k \in [0.93;1.46]$
2	5	$k \in \,]0.01;0.885[$	$R_C \in [1.05,\ 1.75]\,k\Omega,$ this corresponds to $k \in [0.57;0.95]$
3	5	$k \in \,]0.01;0.75[$	$R_C \in [0.98;\ 1.34]\ k\Omega,$ this corresponds to $k \in [0.75;1.02]$

Table 3.3 Synchronization intervals obtained experimentally and through numerical simulation for $\mu=5$ and different degrees of the coupling polynomials.

From Table 3.3, one observes that the decreasing behavior of the synchronization interval as n increases is still present at the same manner as explains above. Figure 3.5 presents an example of phase portraits before the coupling and Figure 3.6 when there is no synchronization while Figure 3.7 presents a state of synchronization.

(a)   (b)
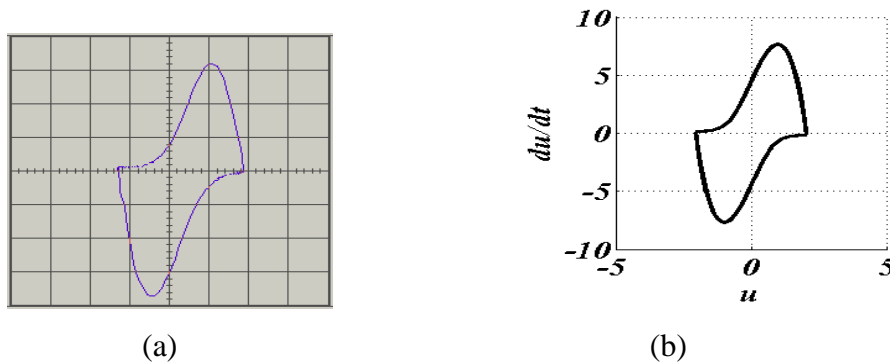
Figure 3.5: Phase portrait exhibited by one oscillator before the coupling. (a) Numerical and (b) Experimental.
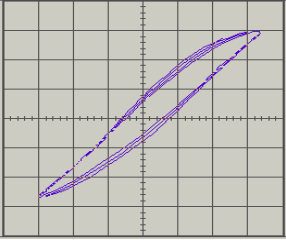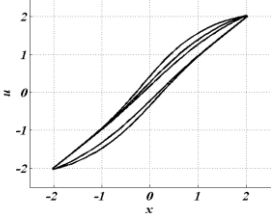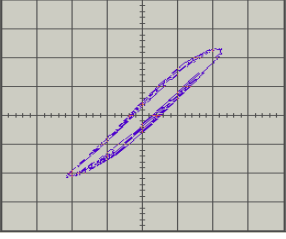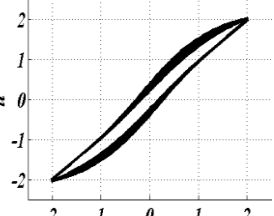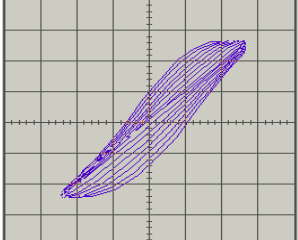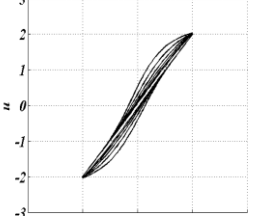
n, k and R_C values	Experimental results	Numerical results
$n=1$ $R_C=30\ k\Omega$, corresponding to $k=0.06$.	 (a)	 (b)
$n=2$ $R_C=24.5\ k\Omega$, corresponding to $k=0.071$.	 (c)	 (d)
$n=3$ $R_C=3.6\ k\Omega$, corresponding to $k=0.5$.	 (e)	 (f)

Figure 3.6 Phase portraits. (a)-(f) are those of coupled oscillators showing the case of no synchronization for different values of parameters *n, k* and R_C in the case of μ=5.
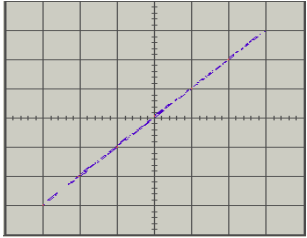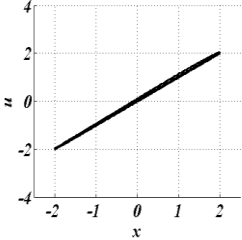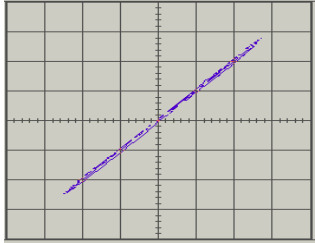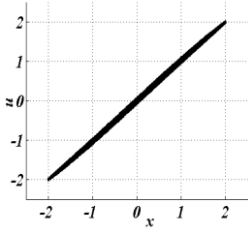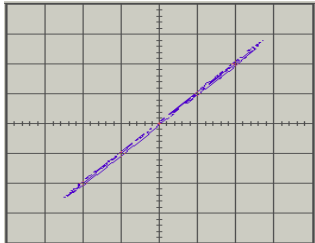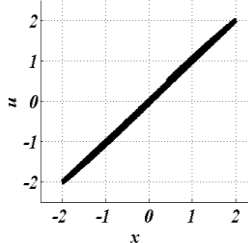
n, k and R_C values	Experimental results	Numerical results
n=1 R_C=60 kΩ, corresponding to k=0.03.	 (a)	 (b)
n=2 R_C=18 kΩ, corresponding to k=0.1.	 (c)	 (d)
n=3 R_C=2.2 kΩ, corresponding to k= 0.82.	 (e)	 (f)

Figure 3.7 Phase portraits. (a)-(f) are those of coupled oscillators showing the case of synchronization for different values of *n*in the case of μ=5.

o **Coupling intervals in the non autonomous case ($E_m \neq 0$).**

According to the parameters obtained in the ref. [35], one can consider these values of Ω excitation: $\Omega \in [2.463, 2.466]$. For example we take $\Omega = 2.465\ Hz$. By setting E= 0.5, meaning $E_m = 5$ V and μ = 5 (see equation (3.4)).

Synchronization occurs in that case for the values of *n* and R_C given in equation (3.9).

$$\forall\, n = \{1,\ 2,\ 3\},\ k \in\,]-\infty;\ -3.5]. \tag{3.9}$$

Figure 3.8 presents the phase plane before the coupling.
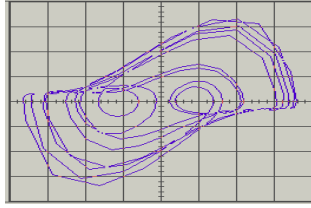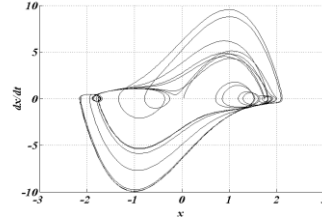
(a)   (b)

Figure 3.8 Chaotic phase portrait exhibited by of each oscillator before the coupling; (a) experiment, (b) numerical simulation.

As before, we check the synchronization state using the phase portraits (x, u). Figure 3.9 presents a state where there is no synchronization while Figure 3.6 corresponds to a state of synchronization. Experimentally, it has been found that there is no clear interval for synchronization for the positive value of the potentiometer *Rc*. Synchronization occurs for some selected values of the resistance. Indeed, by varying *Rc*, one obtains that the chaos synchronization is achieved only for $R_C=0.6 \ k\Omega$, corresponding to *k=1.7*. This is in conformity with the results of Ref. [9] where it was shown that, for positive k, various intervals of synchronization (sometimes limited to a single value) alternate with the no synchronization intervals.
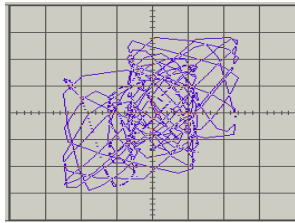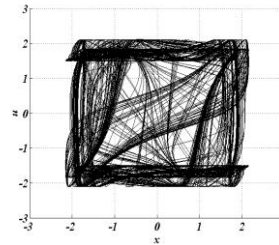
(a)   (b)

Figure 3.9 Phase portrait of the coupled oscillators showing the case of no synchronization for Rc =900 Ω corresponding to *k=1.1*. (a) experiment and (b) numerical.

Figure 3.10 presents the synchronization state for all the values of *n*.
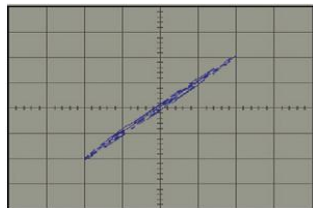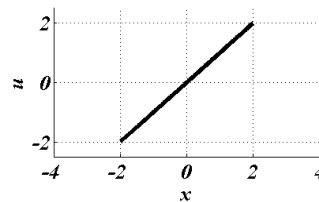
(a)   (b)

Figure 3.10 Phase portrait of the coupled non autonomous oscillators (*with n=3*) showing the case of synchronization for $R_C=0.6 \ k\Omega$ corresponding to *k=1.7:* (a) experimental result, (b) numerical results

III-2-4- Effects of time delay on the synchronization intervals

In this subsection, we will study the effect of delay in the borders of synchronization.

o **Mathematical results**

To better study the mathematical part, one will progressively consider the stability of the synchronization process which develops the Floquet theory and allow us to obtain the Hill equation. To solve this equation and obtain the stable analytical strength parameter, one will use the Whittaker method.

➤ **Stability of the synchronization process**

Considering equation (2.1) where μ is the nonlinear coefficient as we have studied in section I-2-1 and following the procedure explained in chapter 2, one solve Eq (2.25) taking into account the condition (2.26). It is found that the synchronization takes place for

$$k(\tau) \in \left]-\infty, k_1(\tau)\right[\cup \left]k_2(\tau), 1\right[.$$ (3.10)

where
$$
\begin{cases}
k_1(\tau) = \omega^2 \left(-a_{01} - \lambda^2 + n^2 - \sqrt{a_n^2(\tau) - 4n^2\lambda^2} \right), \\
k_2(\tau) = \omega^2 \left(-a_{01} - \lambda^2 + n^2 + \sqrt{a_n^2(\tau) - 4n^2\lambda^2} \right), \\
a_{01} = \frac{1}{\omega^2} \left[1 - \frac{\mu^2}{4} \left(\frac{A^2}{2} - 1 \right)^2 - \frac{\mu^2 A^4}{32} \right], \\
a_n^2(\tau) = a_{ns}^2(\tau) + a_{nc}^2(\tau), \\
\lambda = \frac{\mu}{2\omega} \left(\frac{A^2}{2} - 1 \right).
\end{cases}
$$

o **Experiment results**

To achieve the experiments result of the time delayed coupling system, one use the electrical circuit of figure 3.1(d). Analytical results are obtained by plotting solution (3.10). The numerical one is obtained by plotting Eq. (3.10) using Runge-Kutta 2 delay. According to the experimental results, one built the delayed bloc [73-82] given by figure 3.11.
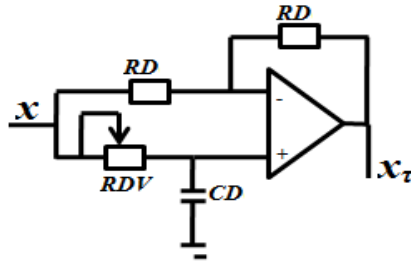
Figure 3.11 Delayed Bloc diagram.

This diagram is constituted by using five components which are one operational amplifier, two resistors, one capacitor and potentiometer, by varying the potentiometer; one obtains different values of the delay. Table 3.4 gives the different values of the parameters.

Résistors (kΩ) Capacitors (nF)	Values
R_D	6.8
R_{DV} (potentiometer)	10.0
C_D	330.0

Table 3.4 Different values of delayed bloc diagram.

To build the values of the delay, one notes $T_D = R_{DV}C_D$; $\tau = \omega_{02}T_D$. By varying the capacitor and using the value $\omega_{01} \approx \omega_{02} \approx 1.16 \times 10^3$ rad/s, one obtains the maximal value of delay: $T_D \approx 3$, 3ms which is the experimental value and it correspond to $\tau \approx 3.828$ for the mathematical and numerical case. To test the efficiency of the bloc diagram, a sinusoidal signal x is sent at the input of the delayed bloc diagram and we measure the output x_τ. Figure 3.12 presents the test results for some selected values of the delay. From the results presented in Figure3.13, it is clear that the bloc diagram is efficient.
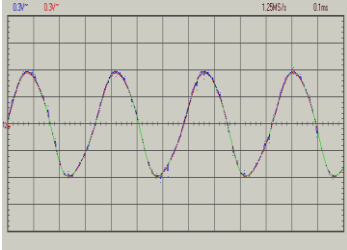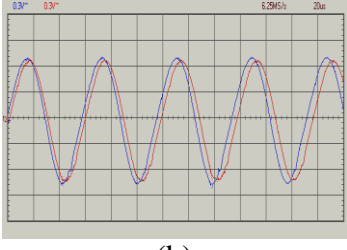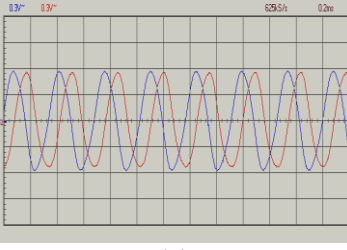
Time delay value and their experiment value	Experiments figures
$\tau = 0$, corresponds to $T_D = 0$ ms	(a)
$\tau = 0.1$, corresponds to $T_D \approx 0.0862$ ms	(b)
$\tau = 1$, corresponds to $T_D \approx 0.862$ ms	(c)

Figure 3.12 Presentation of the delayed bloc diagram and some tests for μ=0.3.

(a) for τ = 0.0, (b) for τ = 0.1 and (c) for τ = 1.

Now using the delayed bloc diagram in the coupling scheme, we have analyzed the effects of the delay on the synchronization interval. These effects appear in Table 3.5 and Figure 3.13. One finds that, experimentally, the borders of the synchronization intervals vary periodically as obtained theoretically. The period of this variation is: $T = \dfrac{3}{2}\tau$.

Values of the delay τ(ms)	Synchronization interval
0	$[0.87;\ 1.53]$
0.1	$[0.81;\ 1.08]$
0.3	$[0.8;\ 0.92]$
0.6	$[0.13;\ 0.16]$
0.9	$[0.1;\ 0.12]$
1.2	$[0.55;\ 0.71]$
1.5	$[1.14;\ 1.19]$
1.8	$[1.11;\ 1.16]$
2.1	$[0.09;\ 0.13]$
2.4	$[0.1;\ 0.18]$
2.7	$[0.42;\ 0.57]$
3.0	$[1.07;\ 1.21]$
3.3	$[1.07;\ 1.17]$
3.5	$[0.62;\ 0.73]$
3.83	$[0.23;\ 0.35]$

Table 3.5 Presentation of the different synchronization intervals for several values of τ.
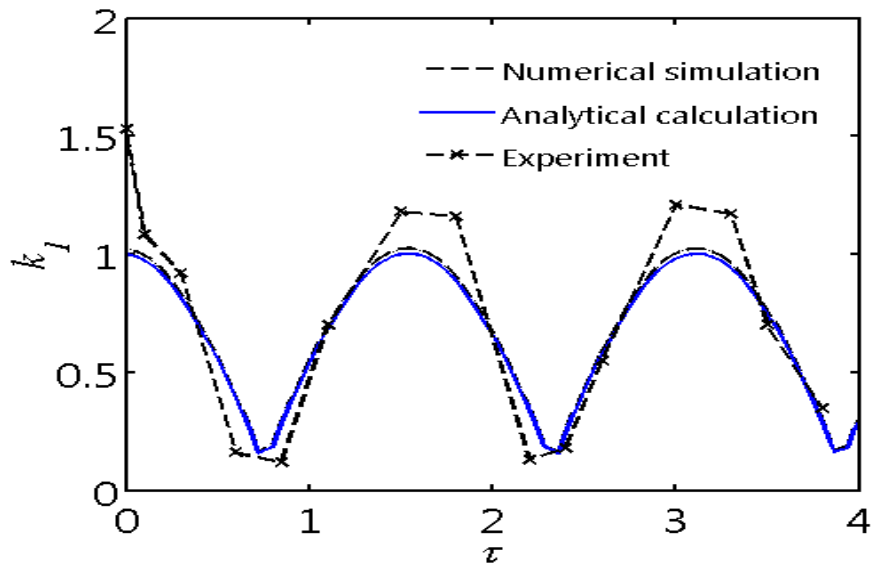
Figure 3.13 Upper boundary of the synchronization intervals versus the delay.

III-2-5- Oscillators subjected to the slowly varying periodic excitations

Van der Pol oscillators submitted to the action of two slowly varying signals present special dynamics consisting of patterns constituted of periodic appearance of packages of periodic/bursting oscillations. These patterns can even show chaotic shape (see Refs.[83–90], for more details). These bursting patterns of electrical nature are interesting as they are special electronic signals, but can also be used to mimic biological signals in artificial devices such as pacemakers. Considering their synchronization is thus of interest and is the subject of this part of the work. The system is described by the following set of equations

$$\ddot{x} - \mu(1-x^2)\dot{x} + x = \delta_1 \cos(\Omega_1 t) + \delta_2 \cos(\Omega_2 t),$$
$$\ddot{u} - \mu(1-u^2)\dot{u} + u = \delta_1 \cos(\Omega_1 t) + \delta_2 \cos(\Omega_2 t) + k(u-x)H(t-T_0),$$

$$(3.11)$$

where the frequencies Ω_1 and Ω_2 are less than 1. δ_1 and δ_2 are positive parameters. We have taken the following values:

$$\delta_1 = 1.1; \ \delta_2 = 0.4; \ \Omega_1 = 0.01; \ \Omega_2 = 0.02. \tag{3.12}$$

For the experiment, the parameters of the excitations are derived from those given in Eq. (3.12) using the following relations.

$$\delta_1 = \frac{R_{12}}{R_{10}} E_{01} \text{ and } \delta_2 = \frac{R_{12}}{R_{10}} E_{02}. \tag{3.13}$$

where E_{01} and E_{02} are the voltage amplitudes coming from each frequency generator. Thus one obtains.

$$E_{01} = 10 \ V; \ E_{02} = 3.7 \ V; \ \Omega_1 = 1.5 \ Hz; \ \Omega_2 = 3.0 \ Hz. \tag{3.14}$$

where ω_1 and ω_2 are the frequencies delivered by the generators. The output delivered by the oscillator subjected to such a signal appears in Figure 3.14 for d=5 and using the parameters in equation 3.28.

Curves	Experiment	Numerical
Time trace	 (a)	 (b)
Phase plan	 (c)	 (d)
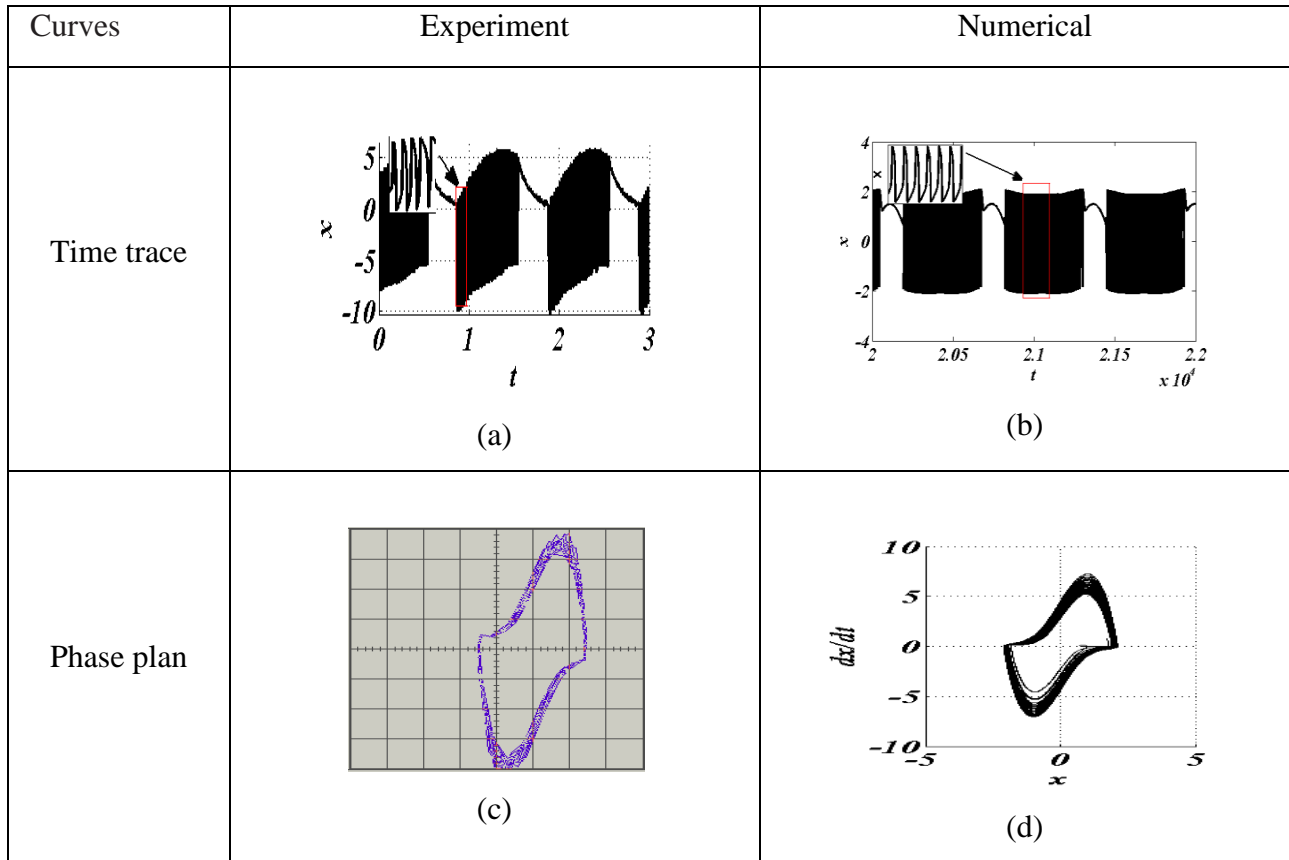
Figure 3.14 Time histories and phase plane exhibited by the oscillators before the coupling. (b) and (d) are numerical results and (a) and (c) are experimental results.

Now, analyzing the synchronization in the case of bursting oscillations, Table 3.6 shows the synchronization domains for μ=5.

Synchronization boundaries obtained from the numerical simulation of Eq. (3.28)	*Synchronizations boundaries obtained from the experiment R_C and (k)*
$k \in [0.3;\ 1]$	$Rc \in [0.830;\ 1.13] k\Omega,$ *this corresponds to* $k \in [0.88;\ 1.21]$

Table 3.6 Synchronization intervals obtained experimentally and through numerical simulation for μ=5.

From Table 3.6, one observes some values of *k* given the boundaries of the synchronization intervals.

III-3- Synchronization and control results using microcontrollers.

In the above sections, the experimental tools have been based on analog simulation. The analog simulation poses some problems related to the choice of the electronic components and the stability of their values. In this section III-3, we use microcontrollers for the same tasks, but with the goal of controlling the oscillator trajectory when it deviates because of some perturbations.

III-3-1- Numerical results.

This section is devoted to the determination of coupling coefficient intervals leading to synchronization using direct numerical simulation.

- ○ **Linear proportional control**

In this case, the dynamics of the Van der Pol with perturbation and coupling scheme is given as follows:

$$
\begin{aligned}
&\ddot{x}_s - \mu(1-x_s^2)\dot{x}_s + x_s = 0, \\
&\ddot{u} - \mu(1-u^2)\dot{u} + u = p(t) + u_1,
\end{aligned}
\tag{3.15}
$$

In this equation, x_s is the reference oscillator and u the actual oscillator which can be submitted to perturbation. u_1 is the proportional control function whose expression is given by

$$
u_1 = kp * e = kp * (x - x_s) \text{ with } e = x - x_s.
\tag{3.16}
$$

where k_p is the coupling coefficient. $p(t)$ is a pulse-like perturbation having the following expression

$$
p(t) = s_1 \sec h\left[s_0 (\omega_0 t - t_i) \right].
\tag{3.17}
$$

where s_1 is the amplitude of the perturbation, s_0 is the pulse width and t_i is the time corresponding to the center of the perturbation. In this work, we use the values $s_1=0.8$, $s_0=1.2$ and $t_i=280$. The natural frequency of the oscillator is fixed to $\omega_0=1$. Figure 3.15 shows the shape of the perturbation as the time evolves. This pulse shape is special as it indicates that the perturbation has a well-known and regular shape. However, it is representative of some types of perturbations that can appear in electrical circuits.
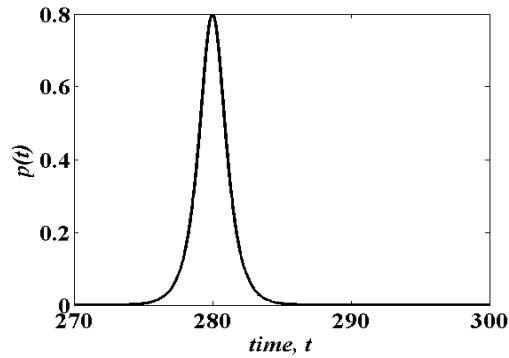
Figure 3.15 Time trace of the perturbation.

When such perturbation hits the actual system described by the variable x, its output is modified in terms of amplitude and phase as it appears in Figure 3.16.   From this figure, one notices the difference of phase introduced by the perturbation. This deviation is harmful for an application where precision is highly required. The values $\mu=0.3$ for sinusoidal output and $\mu=5$ for relaxation output will be used in the rest of the section.

(a)   (b)
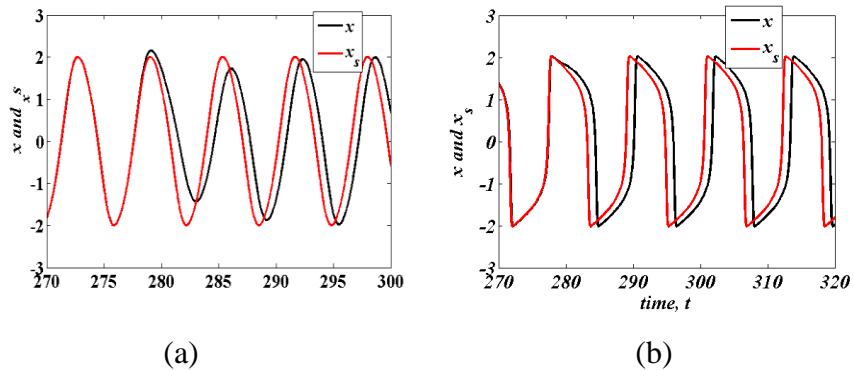
Figure 3.16: Effects of the perturbation on the actual system for a sinusoidal output(a) with $\mu=0.3$ and for a relaxation output (b) with $\mu=5$.

The goal of the coupling scheme is to reduce quickly the deviation in phase and amplitude in order that the actual system returns to its normal operation. The synchronization or the control is thus obtained if the error function e goes to 0 when the time increases. Varying the coupling coefficient k_p, the output of the actual system can either synchronize with the reference system, or not synchronize but remains with its amplitude, or finally, completely change its trajectory. These situations appear in Figure 3.17.
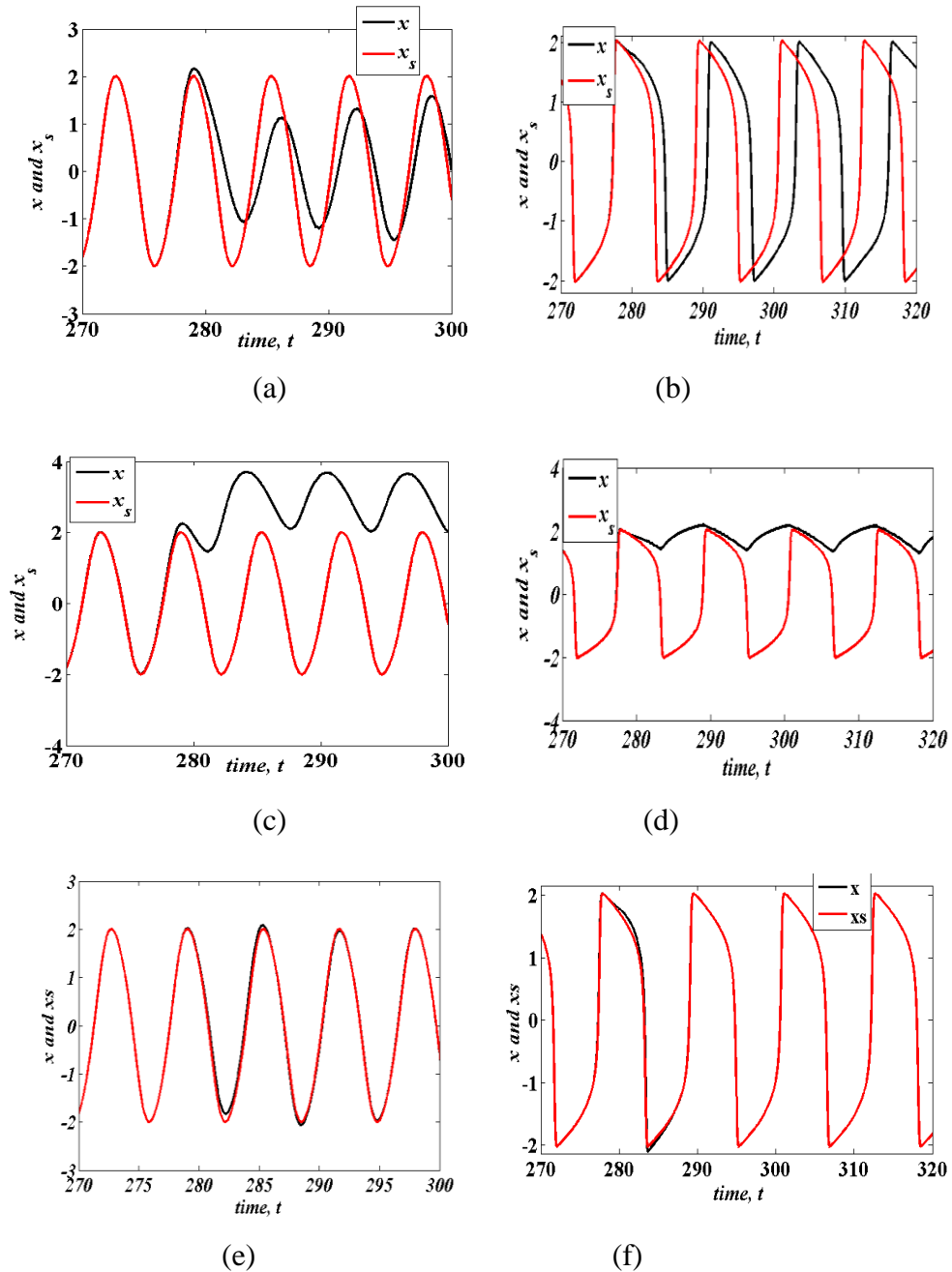
Figure 3.17 Time traces of the system under control showing different outputs for the actual system. (a) and (b): the actual system does not finally follow the reference signal. (c) and (d): the actual system completely changes its trajectory. (e) and (f): the actual system synchronizes with the reference system.

To determine the appropriate control parameters for good control, we have plotted in figure 3.12 the time T_s after which the synchronization is assumed to be achieved. The condition for synchronization is

$$|e| < \varepsilon, \tag{3.18}$$

where ε is the tolerance given by ε=10^{-8}. Ts are plotted versus the coupling coefficient for the case of sinusoidal output (figure 3.18a) and for the case of relaxation output (figure 3.18b).

(a)   (b)
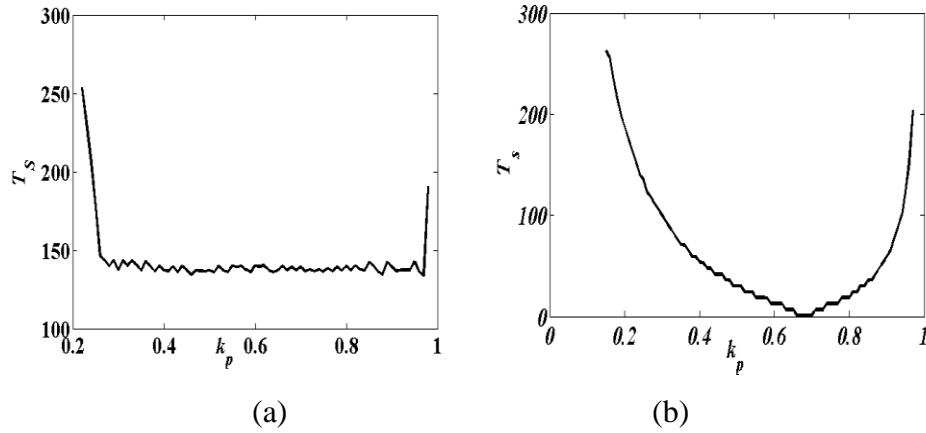
Figure 3.18 Synchronization time versus the coupling coefficient kp. (a) for μ=0.3 and (b) for

μ=5.

From Figure 3.18, the synchronization domain is given by $k_p \in [0.22, \ 0.98]$ for μ=0.3 and $k_p \in [0.25, \ 0.95]$ for μ=5.

o **Proportional control of order *n***

Considering now the case of proportional control of order n, the controller u_1 is replaced by

$$u_2 = k*e = k*(x-x_s)^n,$$ (3.19)

where n is the order of proportional control and k is the coupling coefficient. With this controller, the synchronization time is plotted in Figure 3.19 for three orders of the proportional control for μ=0.3 and μ=5.

(a)   (b)   (c)

(d)   (e)   (f)
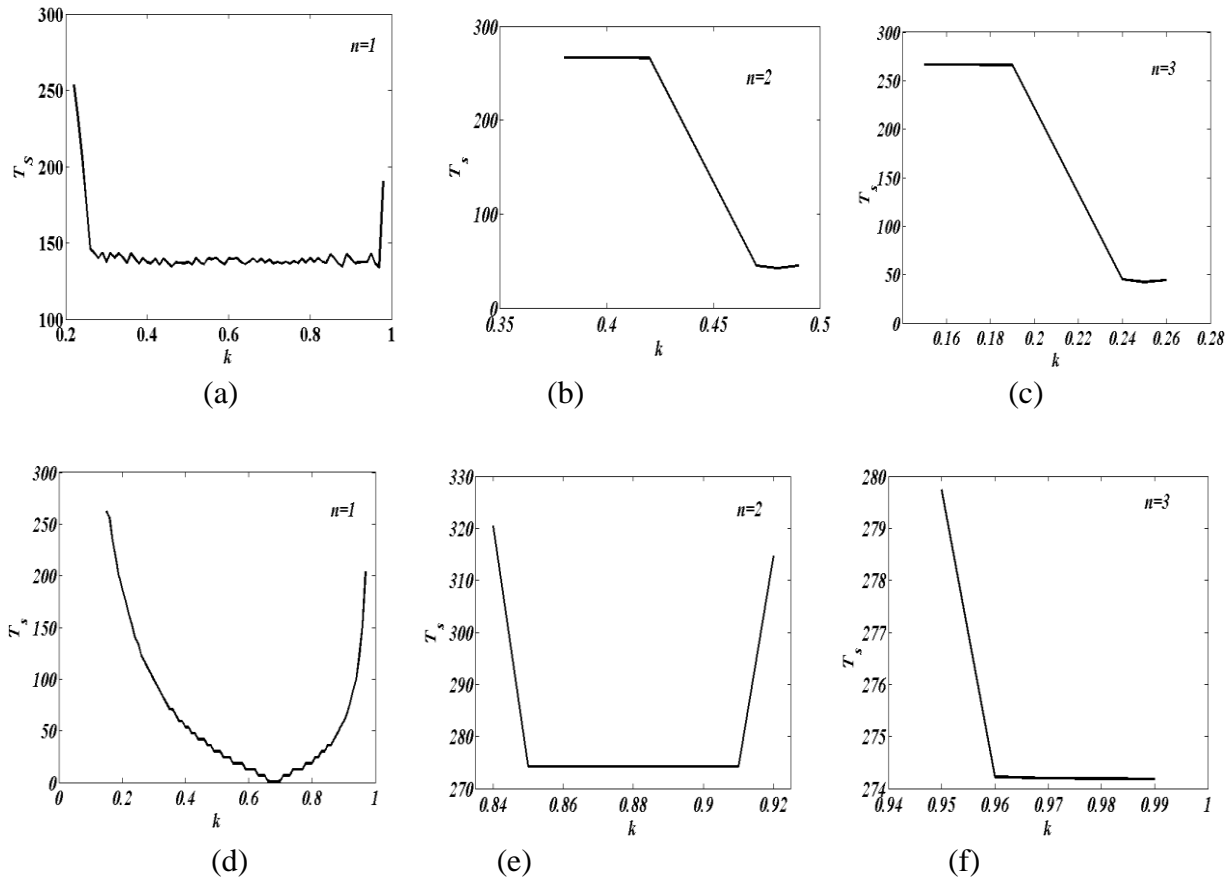
Figure 3.19 Synchronization time of the system under perturbation and control for different orders of the coupling :(a), (b) and (c) for μ=0.3 while (d), (e) and (f) for μ=5.

N	μ	Synchronization domain
1	0.3	$k \in [0.22,\ 0.98]$
2	0.3	$k \in [0.38,\ 0.48]$
3	0.3	$k \in [0.14,\ 0.26]$

(a)

n	μ	Synchronization domain
1	5	$k \in [0.25,\ 0.95]$
2	5	$k \in [0.84,\ 0.92]$
3	5	$k \in [0.95,\ 0.99]$

(b)

Table 3.7 Intervals of the coupling coefficient leading to synchronization for different orders of the proportional control. Fig (a) μ=0.3 and fig. (b) μ=5.

Table 3.7 is obtained from figure 3.13. One notices that when *n* increases, the synchronization domain decreases. Therefore, one can conclude that the linear coupling scheme offers a wider interval for the choice of the coupling coefficient leading to synchronization.

o **Adaptive control**

The principle of adaptive control is that the control gain is a dynamical parameter whose value varies with the time, taking into consideration the deviation between the slave (actual) system and the master (reference) x_s. This is more suitable in situations where some parameters of the system are inaccessible to measurements or can vary with the time. One of the forms of the adaptive controller that will be used here is the following.

$$u_3 = -he,$$ (3.20)

where h is an estimated feedback gain updated according to the following adaptation algorithm

$$\dot{h} = \gamma e^2 \text{ with } h\,(0) = 0.$$ (3.21)

Following the work done in Refs. [91-94], one looks for the suitable values of the coefficient γ which leads the system into synchronization or leads the actual system to converge to the prescribed trajectory x after the perturbation. As in the above sub-sections, this is done by plotting the synchronization time against γ. Figure 3.20 is obtained and shows that synchronization is obtained for γ greater than 0.

(a) (b)
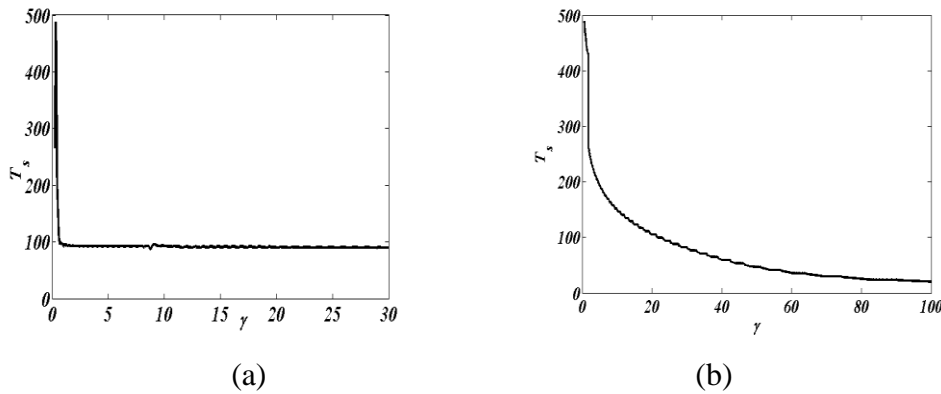
Figure 3.20 Synchronization time versus the adaptive control parameter γ: (a) for μ=0.3 and (b) for μ=5.

Specifically, for μ=0.3, the synchronization interval is $\gamma \in [0.5, \ +\infty[$ while for μ=5, it is $\gamma \in [0.1, \ +\infty[$. The synchronization time decreases when γ increases. Thus, there is an advantage of using the adaptive controller since the synchronization intervals have infinite length in the

positive axis of the control parameter contrary to the proportional coupling schemes for which the synchronization intervals are finite.

To end this subsection, we mention that some of the above numerical results can be obtained from analytical investigation, at least in the case of a sinusoidal trajectory. Some information on this issue can be found in Refs [9] and [95-98].

III-3-2- Implementation in the simple low cost microcontroller

o **Program**

As mentioned in section II, in order to put the equations in a form manageable by the microcontroller, we use the discrete formulation of the equations based on Euler method and write the equations with perturbation as:

$$
\begin{cases}
x_{sj+1} = x_{sj} + p_1 y_{sj}, \\
y_{sj+1} = y_{sj} + p_1 \left[-\omega_0^2 x_{sj} + d\left(1 - x_{sj}^2\right) y_{sj} \right], \\
x_{j+1} = x_j + p_1 y_j, \\
B_j = s_1 \operatorname{sec} h\left(s_0 \omega_0 \left(t_j - t_I\right)\right) = \dfrac{s_1}{1 + \dfrac{\left(s_0 \omega_0 \left(t_j - t_I\right)\right)^2}{2} + \dfrac{\left(s_0 \omega_0 \left(t_j - t_I\right)\right)^4}{24}}, \\
y_{j+1} = y_j + p_1 \left[-\omega_0^2 x_j + d\left(1 - x_j^2\right) y_j + B_j \right].
\end{cases}
\tag{3.22}
$$

where $p_1 = 10^{-3}$ is the time step and B_j is the perturbation. Due to the implementation constraint in the microcontroller, the form of B_j has been developed till order 4. The program is presented in figure 3.21.

```
1-   #include <p18f4550.h>
2-   #pragma config PLLDIV = 5
3-   #pragma config FOSC = HSPLL_HS ,FCMEN = OFF,IESO = OFF, CPUDIV = OSC1_PLL2
4-   #pragma config PWRT = ON,BOR = OFF,BORV = 0
5-   #pragma config WDT = OFF,WDTPS = 32768
6-   #pragma config MCLRE = ON,LPT1OSC = OFF,PBADEN = OFF,CCP2MX = OFF
7-   #pragma config STVREN = OFF,LVP = OFF,XINST = OFF,DEBUG = OFF
8-   #pragma config CP0 = ON,CP1 = ON,CP2 = ON
9-   #pragma config CPB = ON,CPD = ON
10-  #pragma config WRT0 = ON,WRT1 = ON,WRT2 = ON
11-  #pragma config WRTB = ON,WRTC = ON,WRTD = ON
12-  #pragma config EBTR0 = ON,EBTR1= ON,EBTR2 = ON
13-  #pragma config EBTRB = ON
14-  //constants
15-  float d = 0.3;
16-  float s1= 0.8;
17-  float s0 = 1.2;
18-  float ω0=1.0;
19-  float p₁ = 0.001; //Step
20-  float t₁ = 280.;
21-  void main(void)
22-  {
23-  //initial conditions
24-  float x0 = 0.02;
25-  float y0 = 0.03;
26-  float x0s = 0.01;
27-  float y0s = 0.04;
28-  float t0 = 0.0;
29-  float  xs, ys,  x, y, t, A, B;
30-  double pow (double a, double b);
31-  TRISB = 0x00;
32-  TRISD = 0x00;
33-  While(1)
34-  {
35-   t=t0+ p₁;
36-  x = x0 + p₁*y0;
37-  y  = y0  + p₁*(d*(1.-x0*x0)*y0- ω0* ω0*x0);
38-   xs = x0s + p₁*y0s;
39-  A= d*(1.-x0s*x0s)*y0s- ω0* ω0*x0s ;
40-  B=s1/(1.+ pow ((s0* ω0* (t-t₁)), 2) / 2. +pow ((s0* ω0* (t-t₁)), 4) / 24. ); // Disturbance
41-  ys = y0s+ p₁*(A+B);
42-  PORTB = (xs+3)*47.4;
43-   PORTD = (x+3)*47.4;
44-  x0 = x ;
45-  y0 = y;
46-  x0s = xs;
47-  y0s = ys;
48-  t0=t;
49-  }
50-  }
```

Figure 3.21 Program used to program the mickroC PRO for PIC.

From line 1 to 13 is the declaration of the register. From line 14 to 20 is the declaration of the constants. Line 21 presented the starter of the main corps of the executable program. From line 23 to 28, initial conditions declaration. From line 29 to 28, the variables are declared. From line

31 to 32, it is the initialization of the entire pin D and B as the output variables. The while (1) loop of the line 33 gives the started calculation without stopped. From line 35 to 42, expressions of the functions are given. Line 42 and 43 present the ports that the digital calculation results will be loaded. Lines 44 to 48 are the presentation of the closed loop for the repetition functions. From line 49 to 50, the closed loops which are open at starter and while (1).

o **Experimental results**

Simulating the whole program of Figure 3.15 with the software mikroC PRO for PIC and the Proteus software, the outputs of the reference signal ($x(t)$ in PORT D) and the actual signal ($x_s(t)$in PORT B) when there is no perturbation are presented in Figure 3.22.
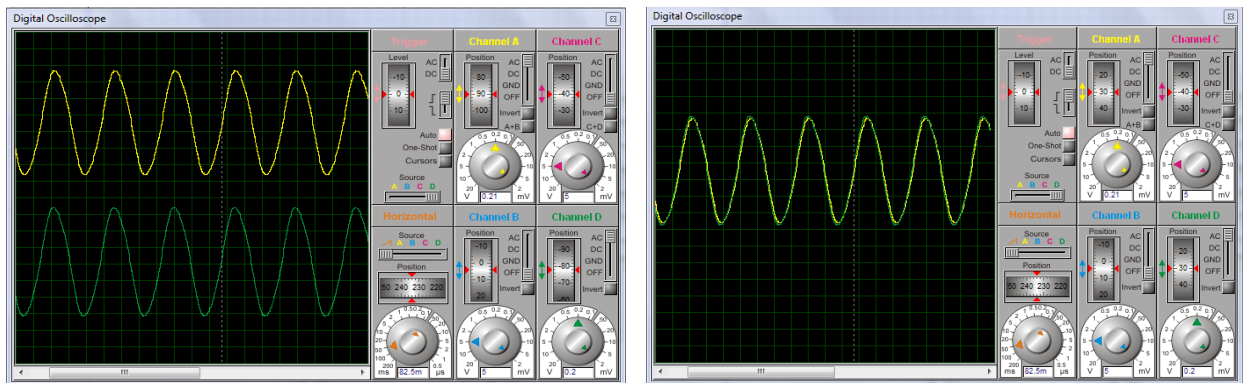
(a)
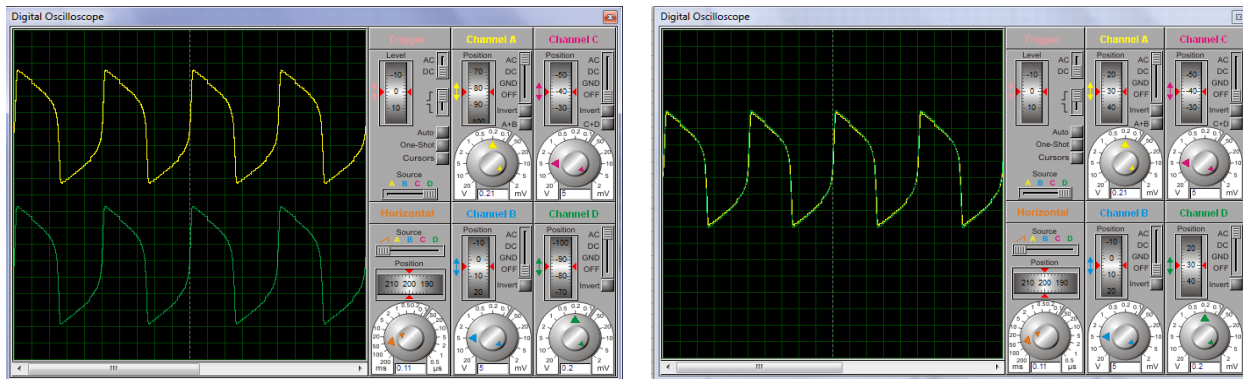
(b)

Figure 3.22 Time traces from the microcontroller of the actual signal x_s (in yellow) and reference signal x (in green) with $s_1=0.0$: (a) for$\mu=0.3$ and (b) for $\mu=5$. The right column corresponds to the superposition of both signals.

Considering now the state where the perturbation is present. The output signals appear in figure 3.23. As it can be observed, the action of the perturbation in the microcontroller version of the

oscillators is similar to what was observed from the experimental simulation: distortion in amplitude and generation of phase difference.
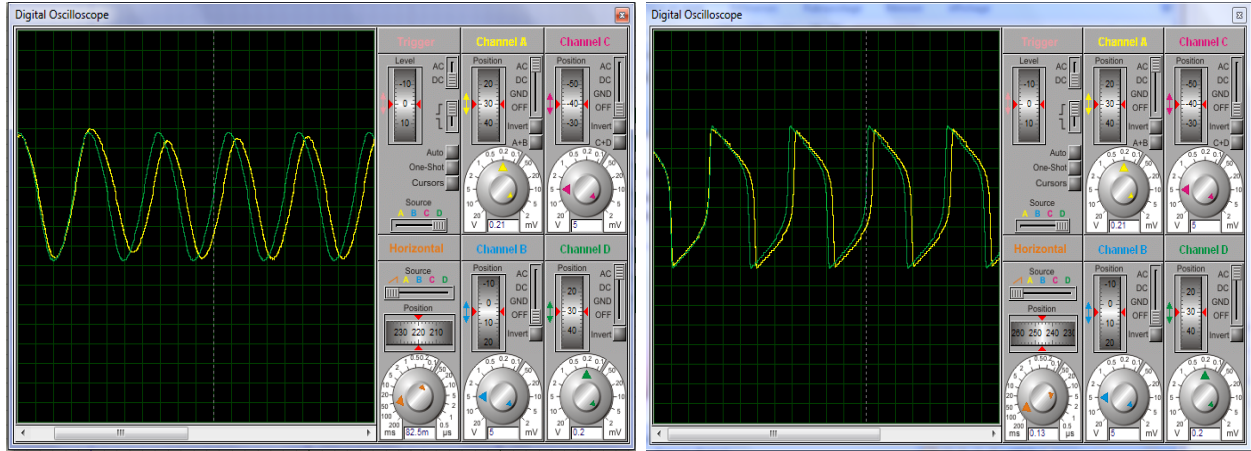
(a)   (b)

Figure 3.23 Time trace of the response generated by the microcontroller when the perturbation affects the actual system: x_s(yellow) and x(green) with $s_1=0.8$ and $s_0=1.2$: (a) for $\mu=0.3$ and (b) for $\mu=5$.

In the case of linear feedback or proportional control case, the discrete form of the controller is

$$u_1 = k_p \left(x_{sj} - x_j \right), \tag{3.23}$$

This term is added in the last equation of the set of equations (6) after multiplying by the discrete time step. Taking $k_p=0.66$, Figure 3.23 shows the effectiveness of the control of the actual system to the reference one (both the results generated by the microcontroller and those obtained from the direct numerical simulation are presented). As concerns the intervals of k_p leading to control, we have obtained that the interval obtained in the numerical simulation also holds for the microcontroller simulation for $\mu=0.3$. But for $\mu=5$, a difference is observed since with the microcontroller simulation, the interval for control is $k_p \in [0.31, \ 0.98]$ for $\mu=5$. This can obviously be explained by the numerical scheme implemented in the microcontroller, but also by the approximation made when implementing the perturbation function in the microcontroller.

In the case of non linear feedback or proportional control case, the discrete form of the controller is

$$u_2 = k \left(x_{sj} - x_j \right)^n, \tag{3.24}$$

The following intervals of the coupling coefficient k leading to control or synchronization are obtained from the microcontroller simulation for $n=3$: $k \in [0.14, 0.26]$ for $\mu=0.3$ and $k \in [0.4, 0.91]$ for $\mu=5$. The experimental results are almost the same as those presented in figure 3.24. Therefore, they have not been presented.
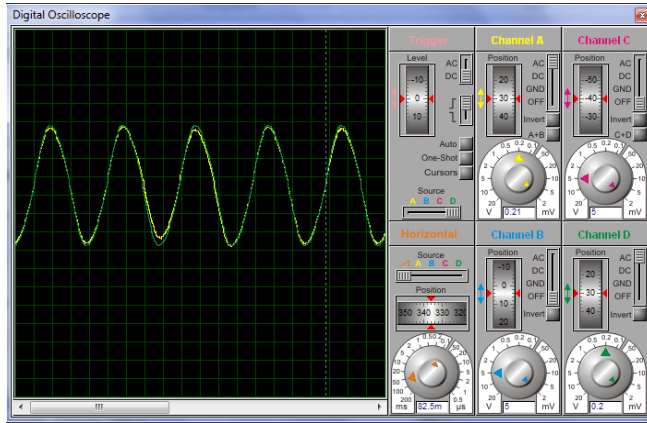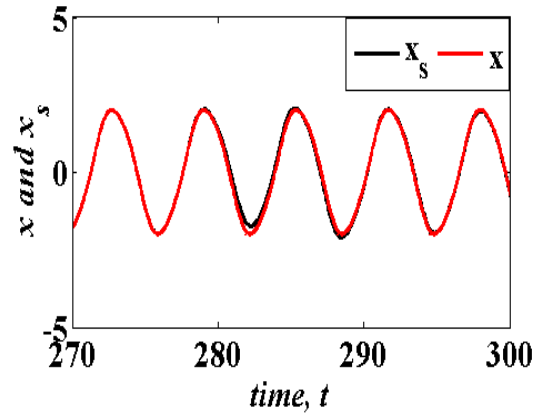
(a) (b)
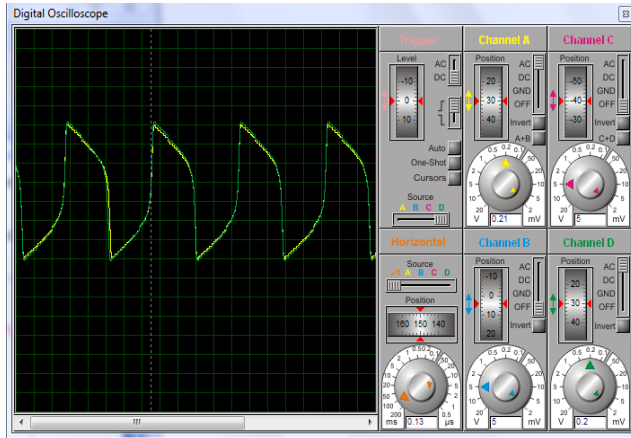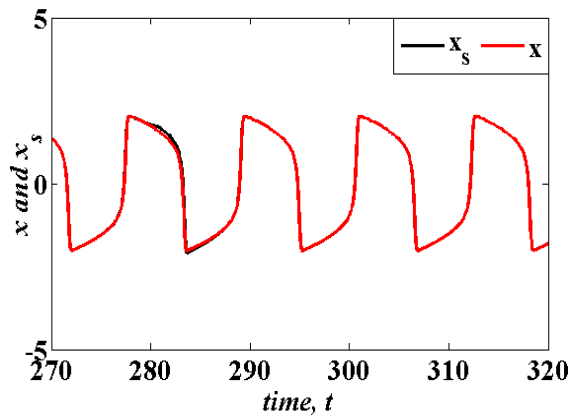
(b) (c)

Figure 3.24 Time trace of the signals when the control is effective for $k_p =0.66$: (a) and (b) for $\mu=0.3$ and (c) and (d) for $\mu=5$.

In the case of the adaptive controller, a new equation is added corresponding to the discrete version of the adaptive controller. This new discrete equation is

$$h_{j+1} = h_j + p_1 \left[\gamma \left(x_{sj} - x_j \right)^2 \right].$$ (3.25)

From this equation the discrete component is given as

$$u_3 = -h_j\left(x_{sj} - x_j\right).$$

(3.26)

This is multiplied by the time step p_1 and added to the last equation of the set of equations (6). The simulation from the microcontroller shows that the synchronization is achieved for γ greater than *0.5* for μ=*0.3* and for γ greater than *0.06* for μ=*5*. These limits are almost equal to those obtained from the numerical simulation. Figure 3.25shows the comparison between experiment and numerical simulation in the case of the adaptive control. It appears that for low value of γ=10, there exists a qualitative agreement between the numerical and experimental results (see Figure 3.25).
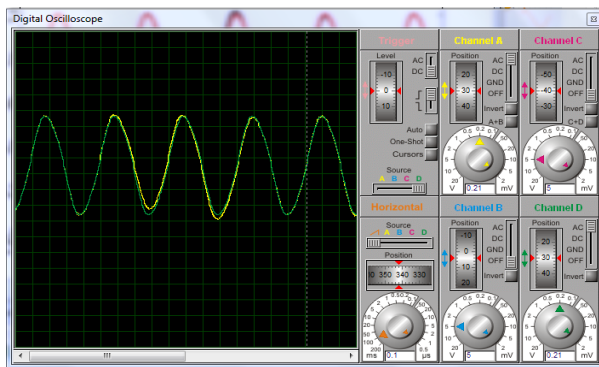
(a)
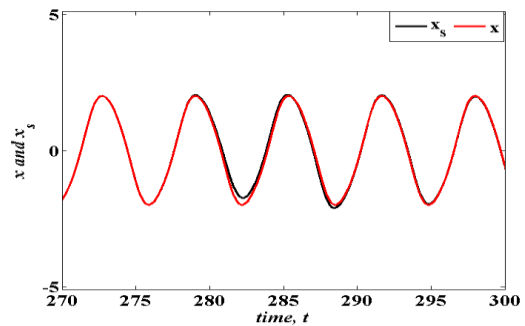
(b)
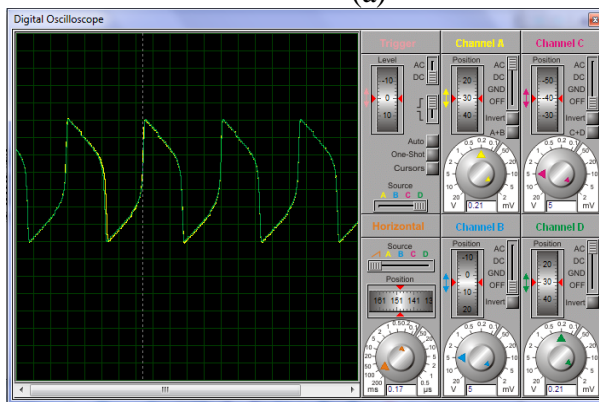
(c)
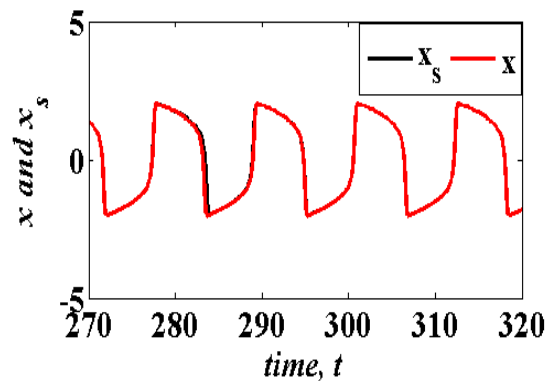
(d)
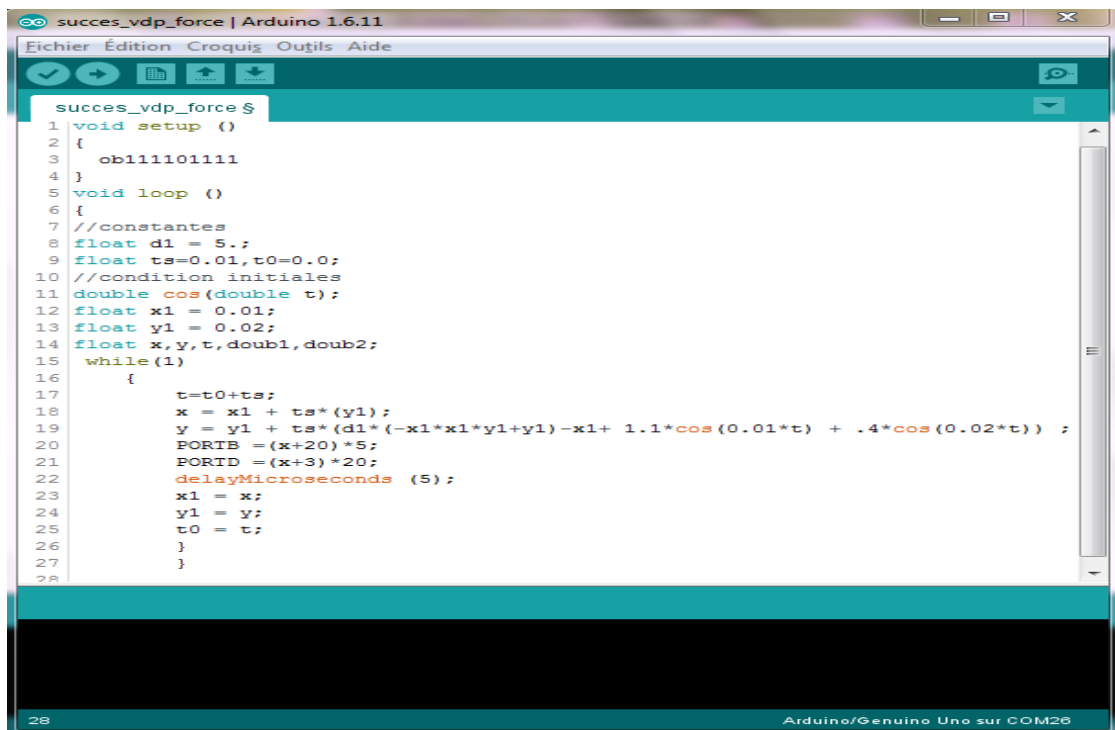
Figure 3.25 Time trace of the signals when the control is effective for γ=*10:* (a)-(b) for μ=*0.3* and (c)-(d) for μ=*5*.

III-4– Fabrication of self-sustained and chaotic signals generator

Most of the time, we usually use the generator bought in the market which produces only basic signals as sinusoidal, triangle, ramp and square. We propose to build a special two voices generator which can be able to produce at the same time, periodic and chaotic signals in different forms. This generator is based on microcontroller.

III- 4-1- Basic information to produce analogical signals using microcontroller

Programming microcontroller and producing the analogical signal, is presented in this subsection. First we need to have one computer inside which we install the mikro C pro for PIC to programme or Arduino interface. We need also to have the picIt 3 to charge the programmed signal inside the microcontroller passing through the USB cable. Two coaxial cables must be used to observe the electronic signal inside the oscilloscope. Different figures below present these statements by using Arduino uno board. Figure 3.26 presents the screen capture of the programmable interface inside the computer.


```
succes_vdp_force | Arduino 1.6.11
Fichier  Édition  Croquis  Outils  Aide

  succes_vdp_force §
 1 void setup ()
 2 {
 3   ob111101111
 4 }
 5 void loop ()
 6 {
 7 //constantes
 8 float d1 = 5.;
 9 float ts=0.01,t0=0.0;
10 //condition initiales
11 double cos(double t);
12 float x1 = 0.01;
13 float y1 = 0.02;
14 float x,y,t,doub1,doub2;
15  while(1)
16    {
17        t=t0+ts;
18        x = x1 + ts*(y1);
19        y = y1 + ts*(d1*(-x1*x1*y1+y1)-x1+ 1.1*cos(0.01*t) + .4*cos(0.02*t)) ;
20        PORTB =(x+20)*5;
21        PORTD =(x+3)*20;
22        delayMicroseconds (5);
23        x1 = x;
24        y1 = y;
25        t0 = t;
26    }
27    }

28
                                                    Arduino/Genuino Uno sur COM26
```

Figure 3.26 Capture of the programmable interface inside the computer.

After programming the function, we load it inside the microcontroller by using the USB cable connected as in Figure 3.27.

Figure 3.27 Presentation of connecting USB cable.

After connecting this USB (universal serial bus) cable, the signal can be loaded inside the microcontroller. Signal loaded in the microcontroller is the digital one. To convert to the analogical one, one will use the analogical converter. We use the passive converter which contains only the resistors and is very efficient. Figure 3.28 presents that converter called the R-2R converter. It is a network of resistors.
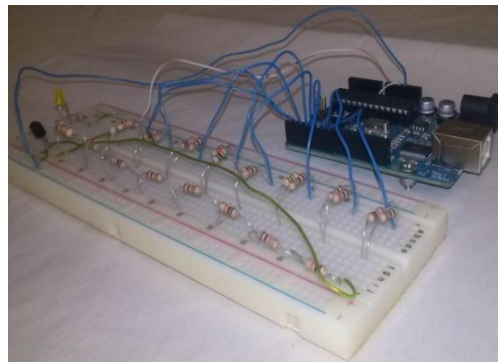
Figure 3.28 The R-2R converter in laboratory connected to the Arduino uno.

The current starts passing through the R and is divided by the 2R. At the end, one obtains the simple analogical signal. According to this information, one can built a lot of signals using the differentials equations. One programs the different signals as given down below. The left figure present the simple test of the system programmed by using the function $A(t)$ given below

$$A(t) = 1.25 * \sin(0.25 * t).\tag{3.27}$$

The right one presents the excited Van der Pol oscillator as following:

$$\frac{d^2x}{dt^2} + \mu(x^2-1)\frac{dx}{dt} + x = f_{01}\cos(\omega_1 t) + f_{02}\cos(\omega_2 t).$$ (3.28)

with the following values of the constants:

$f_{01}=1.1,\ f_{02}=0.4\ \omega_1=0.01,\ \omega_2=0.02\ and\ \mu=4.$ (3.29)

Figure 3.29 presents the output of the equations (3.27) and (3.28).
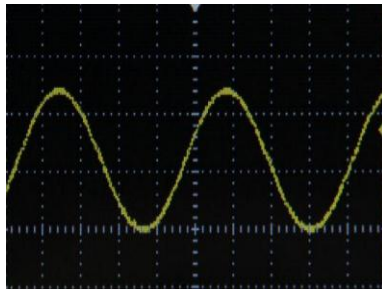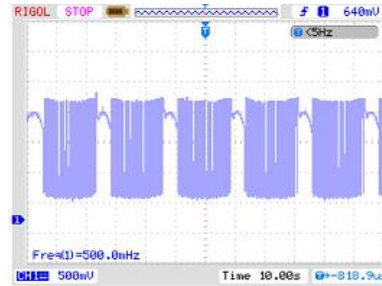
(a)   (b)

Figure 3.29 Time trace of the functions (a) $A(t)$ and (b) forced Van der Pol oscillator.

With all these competences, we build a generator which can be used to generate electrical signals in different forms.

III-4-2-Structure of the generator

To better present the structure of the generator, one will start by presenting the inside of the generator. Here the different components and their functions will be presented. Then in the outside, on the face, one will present also the different parts and their corresponding functions.

o **Internal structure of the generator.**

This new generator is built by using the new type of microcontroller called the ATMEGA 32. It has some capacities different to the others. As we have presented in the case of the PIC 18F4550, this ATMEGA 32 microcontroller has a very high velocity capable to execute the very large instructions at the same time. It is easy to program AVR controller [99-100]. With appreciable program memory it can satisfy most embedded systems. With various sleep modes it can work on mobile embedded systems. Along with 32 programmable Input/output pins, it can interface many peripherals easily. With watchdog timer to reset under error it can be used on

systems with no human interference. Figure 3.30 presents the pins image and some basic characteristics of this faster microcontroller [99-102].

I/O and Packages

– **32 Programmable I/O Lines**

– **40-pin**

• **Operating Voltages**

– **2.7V - 5.5V for ATmega32L**

– **4.5V - 5.5V for ATmega32**

• **Speed Grades**

– **0 - 8MHz for ATmega32L**

– **0 - 16MHz for ATmega32**

• **Power Consumption at 1 MHz, 3V, 25·C**

– **Active: 1.1mA**

– **Idle Mode: 0.35mA**

– **Power-down Mode: < 1µA**
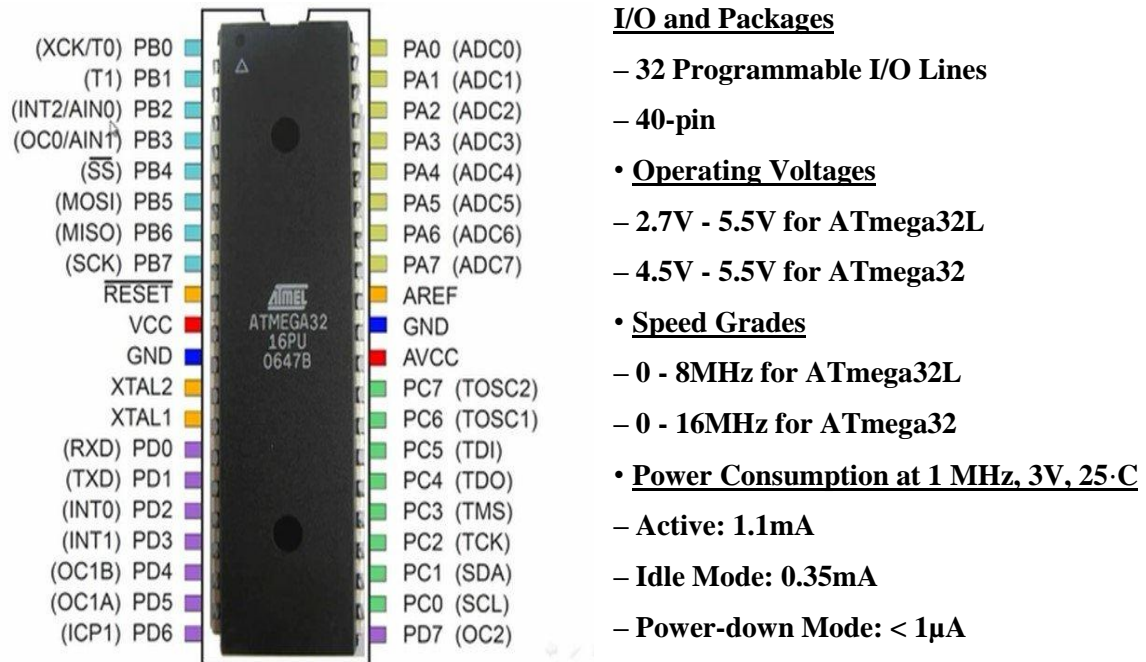
Figure 3.30 ATMEGA 32 and some basic characteristics.

The interface electronic circuits of the generator are given in figure 3.31 below with presented the electronic circuit blocks used to build the generator.
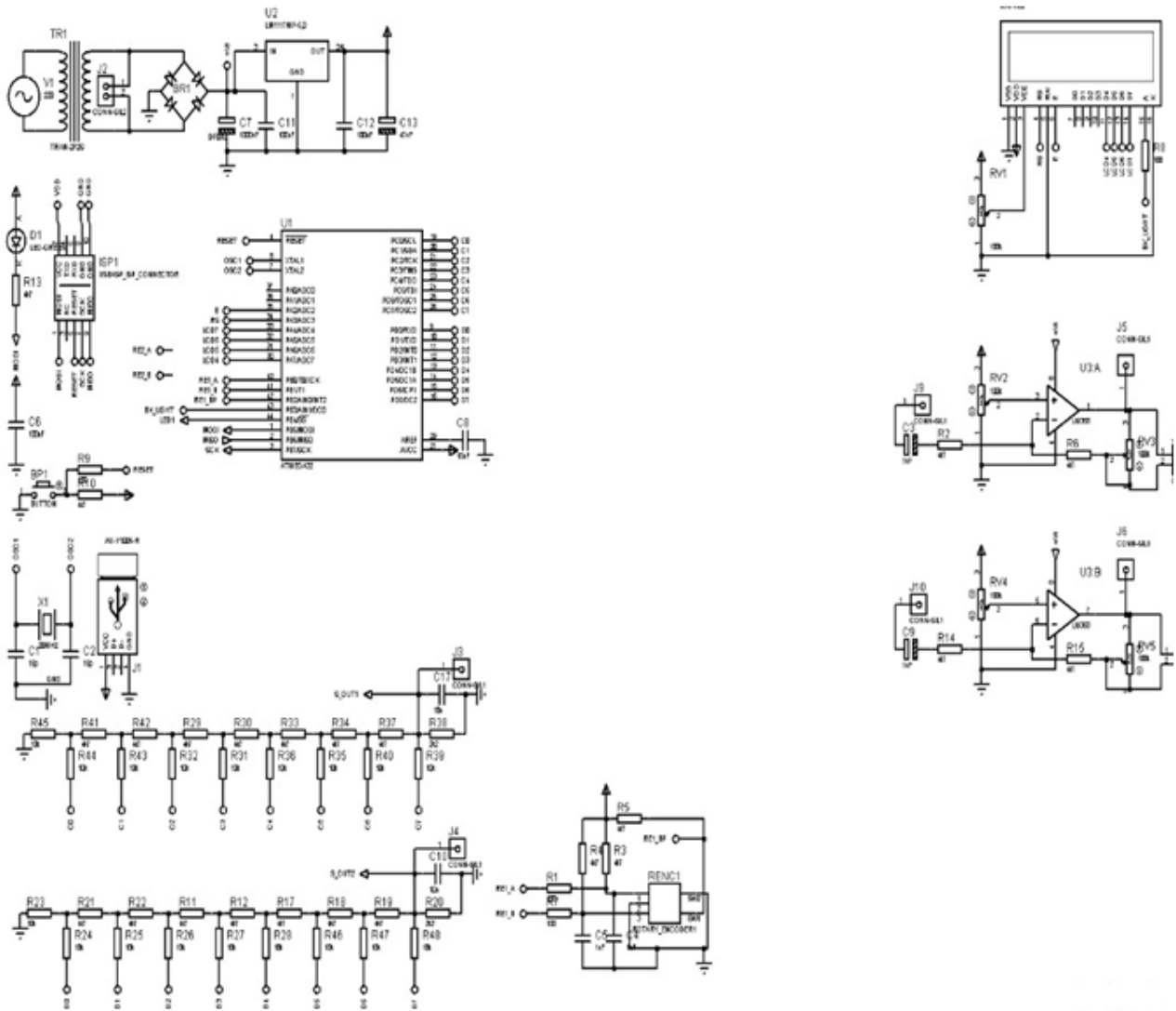
Figure 3.31 Electrical circuit schema of the generator.

Figure 3.31 presents the different blocs used to build the generator. In this figure, for the left side, the first block is the alimentation, the second are: polarization connexion, pulse with modulator, reset bottom and microcontroller. The third one is the circuit of quartz oscillator and the Universal Serial Bus keys connexion. The fourth circuit are the blocs of the digital analogical converter and the filter oscillator of the converted signal. In the right side, the screen and the two identical circuits used to assure the output connexion with the cable to produce the signal to the oscilloscope. In Figure 3.32, one presents the real block connexion used to build the generator.
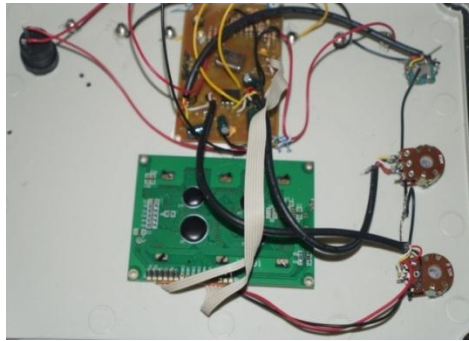
Figure 3.32 Electronic circuits inside the generator.

The green block contains the screen and some resistors of protection. The brown one contains all the building electrical circuit that we have mentioned before. Around these entire connexions, we have the potentiometers and the electrical cables.

o **External structure of the generator**

We present the image of the external structure and explain the role of each part. Figure 3.33 presents the special generator.
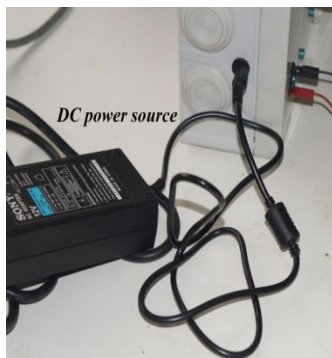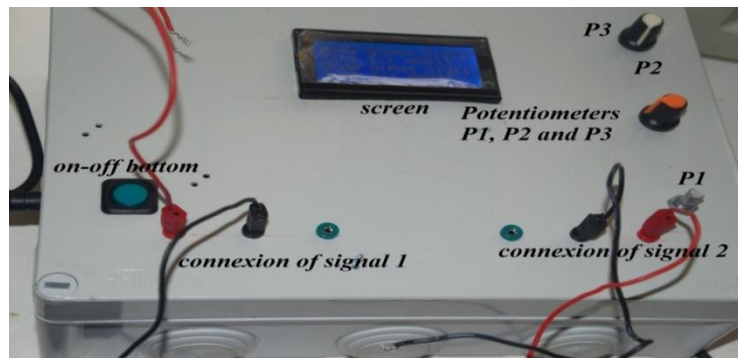
(a)   (b)

Figure 3.33 Presentation of the external structure of the signal generator. (a) External power and (b) External command.

Particular information related to this generator is that: the two connexions signal can function at the same time. In Figure 3.33, we have the direct current power source 5V to power the generator. Then on the main box, we have the on-off bottom used to cut and send the electrical signal inside the generator. The screen is to visualise the characteristics of the signal choice as the Figure 3.34 presented.

Figure 3.34 Screen of the generator**.**

G is the gain of amplitude when the signal is delivered. It can be varied according to the intention of the user by using the potentiometer P3.Ts is the frequency of the coming out signal. This can also be varied by using potentiometer P2. The type of signal is changed by using potentiometer P1. In the signal connexions, there exist two ports. Signals 1 and 2 have three output voice which are red, black and green. The combination of red-black gives the simple permanent signal in the one calibrated amplitude. The simple variation in that case is only on the frequency. The combination green-black gives the amplitudes and the frequencies variation. Some tests and applications of this generator are presented in the following section.

III-4-3-Signals produced by the generator

The aim here is to present the efficiency of the generator. We start first by presenting the different tests of the generator in the laboratory. Figure 3.35 presents the tests in the laboratory.
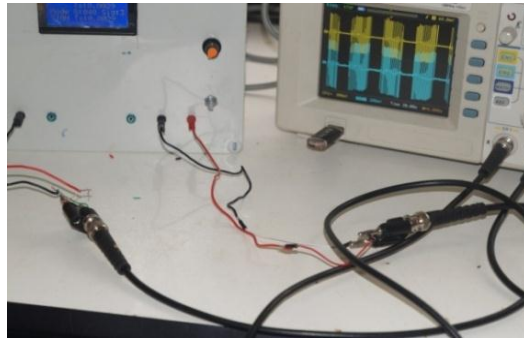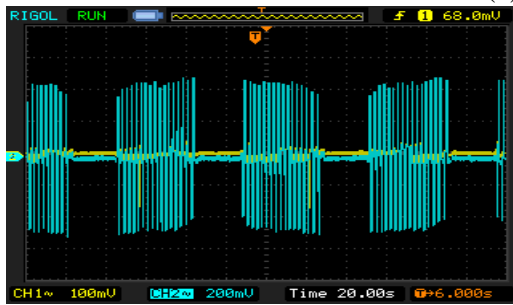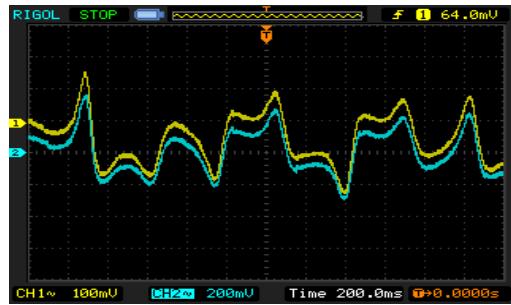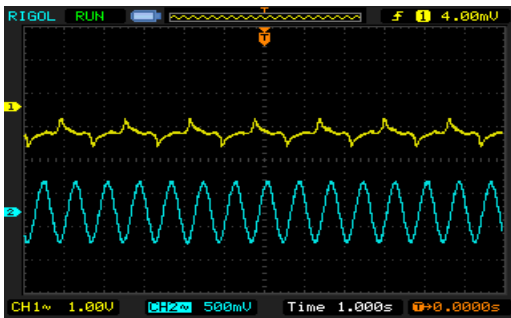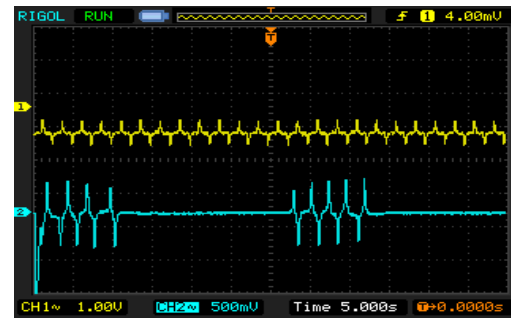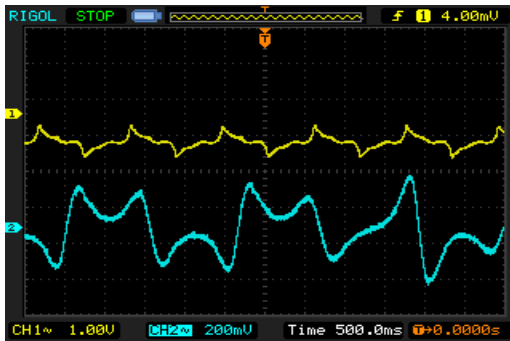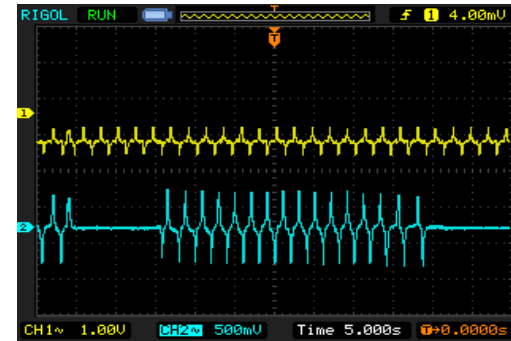
Figure 3.35: Different time traces of the Van der Pol oscillator and the Lorentz chaotic signal (a) generator with the two voices, from (b) to (g) signal coming from Van der Pol oscillator(autonomous and excited).

Fig. 3.35 (b) presents Van der Pol oscillator mixed. Fig.3.35 (c) presents the chaotic dynamics with the parameters taken in Ref [35]. Fig.3.35 (d) presents the small frequency and amplitude bursting and Van der Pol (for μ=0.3) oscillations. Fig.3.35 (e) exhibits the high frequency and small amplitude of bursting in the states of periodic mixed mode oscillations. Fig.3.35 (f) presents the high amplitude of chaotic dynamic and small amplitude and frequency of bursting oscillations and Fig.3.35 (g) shows small amplitude of periodic and high one for chaotic bursting oscillations.

III-5- Conclusion

In this chapter, we have presented the mathematical results, numerical results, analog results through the electronic circuits, microcontroller results of two coupled Van der Pol oscillators and built a generator which can be used to power any type of devices. Firstly, we have solved analytically delayed coupled Van der Pol oscillators and simulated numerically and analogically delayed Van der Pol oscillators. The results obtained were in good agreement. Secondly, we have presented the microcontroller simulations of the coupled Van der Pol oscillators subjected to disturbances and the results were in agreement with the numerical simulations. Thirdly, we have built a generator which produce complex signals and. These constitute the main achievements of the thesis.

General Conclusion

The main aims of this thesis were four folds: firstly, to determine experimentally the suitable synchronization coupling coefficients of two coupled Van der Pol electrical oscillators subjected or not to the periodic excitation. Secondly to use microcontrollers for the digital implementation of the control of two coupled Van der Pol electrical oscillators subjected to disturbances. Thirdly, to build a generator based on the microcontroller component and some different electrical circuits.

Summary of the main results

For the first aim, the question of an experimental determination of synchronization intervals in the case of two Van der Pol oscillators coupled unidirectional nonlinear coupling function and through a linear coupling with delay has been analyzed. Three states of excitation have been considered: autonomous system, excitation with a single periodic signal leading to chaos and excitation with two slowly varying sinusoidal components leading to bursting oscillations. The synchronization intervals have been determined and it has appeared that they are reduced when the degree of the polynomial coupling function increases. Moreover, in general, an agreement has been found between the experimental investigation, the numerical simulation and the analytical calculation. It has been found that the synchronization time reduces when the degree of coupling polynomial increases. In the case of the coupling the delay, the experimental results have confirmed the sinusoidal dependence of the critical coupling for synchronization as predicted by the theory (analytical and numerical simulations predictions).

For the second aim, the problem of the synchronization of Van der pol oscillators submitted to the disturbances using a microcontroller has been considered. Three control schemes have been used: linear proportional control, nonlinear proportional control of order n and adaptive control function. The synchronization intervals have been found from the numerical simulation by plotting the synchronization time. It has been found that the adaptive controller shows an infinite range for the control parameters leading to control contrary to the proportional controllers which present a very limited range of the control parameters. The implementation inside the microcontroller using the software mikroC PRO for PIC has been used. The results coming from the microcontroller demonstrate that it is an efficient way to produce and

synchronize self-sustained electrical oscillations. The synchronization intervals have been determined from the simulation based on microcontroller and it has been found an interesting agreement with the numerical simulation.

Thirdly, from the expertise acquired from the microcontroller simulation of differential equation, we have built a generator which produce periodic and chaotic signal.

Further Works

In this thesis, some interesting results have been obtained and have opened interesting perspectives for the further investigations.

The further works that could be based on this thesis are:

1. From the experimental studies of the synchronizations of two Van der pol electrical oscillators, it should be interesting to study feedback coupled Van de Pol oscillators with double delays (master and slave) using analog and microcontroller components.

2. According to the large knowledge acquired in the field of microcontrollers which has been permitted to program the DEs, one can program fractional order DEs using microcontrollers and use the signal to power a ring of electromechanical systems.

3. Using microcontroller as the experimental component which produce only nonlinear effect of the DE and will be associate to the others electrical components of the circuit to produce the final signal of the DE.

Bibliography

[1] L. M. Pecora and T.L. Carroll, Phys. Rev. Lett., 64, 821, (1990).

[2] T. Kapitaniak, Phys. Rev. E, 50, 1642-1644, (1994).

[3] H. Fotsin and S. Bowong, Chaos Solitons Fractals, 27, 822-835, (2006).

[4] C. Juan, L. Jun-An and W. Xiaoqun, J. Syst. Sci. Complex, 24, 433-448, (2011).

[5] P. E. Yu and A. P. Kuznetsov, Tech. Phys, 56, 435-442, (2011).

[6] S. T. Kingni, S. Jafari, H. Simo and P. Woafo, Eur. Phys. J. Plus, 76, 120-129, (2014).

[7] M. A. Barron, J. Appl. Res. Tech., 14, 62-66, (2016).

[8] F. Alderisio, B.G. Bardy and M. Di Bernardo, Biol Cybern. DOI:10.1007/s00422-016-0685-7, (2016).

[9] P. Woafo and R.K. Kraenkel, Phys. Rev. E., 66, 25-31, (2002).

[10] B. Nana and P. Woafo, Phys. Rev. E., 74, 046-213, (2006).

[11] B. Nana and P. Woafo, Ajeee, 3, 37-43, (2015).

[12] S. Sabarathinam and K. Thamilmaran, J. Appl. Phys, DOI:10.9790/4861-17002012633, (2017).

[13] Y. Chembo Kouomou and P. Woafo, Phys. Lett.A, 298, 18-28, (2002).

[14] R. Yamapi, O. Chabi and P. Woafo, Int. J. Bifurcation Chaos, 14, 171-181, (2004).

[15] N. Buric and N. Vasovic, Chaos Solitons Fractals, 31, 336-342, (2007).

[16] K. Srinivasan, D.V. Senthilkumar, K. Murali, M. Lakshmananand J. Kurths, Chaos, 21, 023-119, (2011).

[17] J. Sawicki, M. Abel and E. Scholl, Cybern. Phys., 4, 112-115, (2015).

[18] L. Lazarus, M. Davidow and R. Rand, Procedia IUTAM, 19, 152-160, (2016).

[19] A. P. Fournaris and N. Sklavos, Comput. Elect. Eng. 40, 121–133, (2014).

[20] A. A. Elbaset, A. Hamdi, M. Abd-El Sattar and M. Khaled, IET Renew Power Gen. 10, 551–560, (2016).

[21] M. A. Murillo-Escobar, C. Cruz-Hernández, F. Abundiz-Pérez and R. M. López-Gutiérrez. Microprocess. Microsyst. 45, 297–309, (2016).

[22] S. Kaçar. Opti-Int. J. Light. Opt. doi:10.1016/j.ijleo.2016.07.044, (2016).

[23] J. Chandramohan, R. Nagarajan, K. Satheeshkumar, N. Ajithkumar, P. A. Gopinath and S. Ranjithkumar. Int. J. Eng. And Comp. Sci. 6, 20694–20698, (2017).

[24] Y. Raghavender Rao. Int. J. Eng. Tech. Sci. Res. 4, 2394–3386, (2017).

[25] R. Chiu, M. Mora-Gonzalez and D. Lopez-Mancilla. Eng. Comput. Science, IERI Procedia. 4, 247–252, (2013).

[26] M. Z. De la Hoz, L. Acho and Y. Vidal. Scientif. World J. 10, doi:10.1155/2015/123080, (2015).

[27] H. Hamiche, S. Guermah, R. Saddaoui, K. Hannoun, M. Laghrouche and S. Djennoune, Nonlinear Dyn. 8, 1921–1932, (2015).

[28] A. S. Andreatos and C. K. Volos.11, 023-34, (2014).

[29] M. A. Murillo-Escobar, C. Cruz-Hernández, F. F. Abundiz-Pérez and R. M. López-Gutiérrez. Expert Syst. Appl. 42, 8198–8211, (2015).

[30] E. W. Chimi Kontchou, H. B. Fotsin and P. Woafo. Phys. Scr. 77, 045– 001, (2008).

[31] B. Van der Pol. Radio Review, 1, 701–710, 754–762, (1920).

[32] B. Van der Pol. Phil. Mag., 2, 978–992, (1926).

[33] B. Van der Pol. Phil. Mag., 3, 6-4, (1927).

[34] B. Van der Pol and J. van der Mark. Phil. Mag. 6. 763. (1928).

[35] U. Parlitz and W. Lauterborn, Phys. Rev. A, 36, 1428-1434, (1987).

[36] H. G. Winful and L. Rahman. Phys. Rev. Lett. 65, 1575, (1990).

[37] L. O. Chua. 46, 250, (1992).

[38] P. F. Rowat and Allen I. Selverston, journal of neurophysiology 70,3, (1993).

[39] J. Cartwright, V. Eguiluz, E. Hernandez-Garcia, and O. Piro, 9, 2197–2202, (1999).

[40] V. Balachandran and Kandiban. Ind. J. P. Appl. Phy, 47, 823-827, (2009).

[41] E. N. Lorenz. J. Atmos. Sci. 20,130, (1963).

[42] A. S. Pikovsky. Sov. J. Commun. Technol. Electron. 30, 10, (1985).

[43] H. Kawakami and R. Lozi.18, 145-150, (1992).

[44] H. Nijmeijer, I. M. Y. Mareels. IEEE TCAS-I. Fund. Theor. Appl. 44, 10, (1997).

[45] S. Agarwal. Master's thesis, July, (2002).

[46] L. Zhi and H. C. Zhao. Chinesse Phys. 11, 666, (2002).

[47] J. J. E. Slotine, W. Wang, and K. El Rifai. Proceedings of the 6th International Symposium on Mathematical Theory of Networks and Systems, Katholieke Universiteit Leuven, Netherlands, Jul. 9, (2004).

[48] Z. Li and G. Chen. Phys. Lett. A. 324, 166, (2004).

[49] H.G. Enjieu Kadji, J.B. Chabi Orou, P. Woafo. CNSNS, 1007-5704, (2006).

[50] R. Yamapi, P. Woafo. CNSNS. 11, 186 – 202, (2006).

[51] R. Yamapi and M. A. Aziz-Alaoui. CNSNS 12, 1534–1549, (2007).

[52] G.S Mbouna Ngueuteu, R. Yamapi and P. Woafo Communications in Nonlinear Science and Numerical Simulation 13, 1213–1240, (2008).

[53] E. Tafo Wembe and and R. Yamapi, CNSNS. 329, 3137–3148, (2008).

[54] R. Yamapi and P.Woafo, JSV, 285, 1151-1170, (2005) Systems and Control Conference, DSCC, (2013).

[55] H. B. Fotsin and P. Woafo, chaos, soliton and fractal, 24, 1363-1371, (2005).

[54] R. Yamapi, B.R. Nana Nbendjo, H.G. Enjieu Kadji Int. J. Bif.chaos 17, 1343–1354, (2007).

[57] 'https://www.microchip.com/architecture_microcontroller_pic'

[58] 'https://www.google.com/image/*_road_using%compiler%micro'

[59] 'https://fr.wikipedia.org/wiki/Microcontr%C3%B4leur_PIC'

[60] H. Hamiche, M. Ghanes, J.P Barbot, K. Kemih and S. Djennoune. 20, 99-113,(2013).

[61] E. Butcher, A. Sinha. Nonlinear dynam. 17, 11-21, (1998).

[62] A. H. Nayfeh and D. T. Mook.Wiley- Interscience, New York,(1964).

[63] R. Thepi Siewe, A. F. Talla and P. Woafo. Int. J. Nonlin., Sci and Num. Sim. 18 (6), 513-523, (2017).

[64] H. K. Leung, Phys. Rev. E 58, 57-04, (1998).

[65] H. K. Leung, Physica A 281, 3-11, (2000).

[66] P. Frolkovič. 19, 3, Cambridge University Press, (1990).

[67] W. H. Press, S. A. Teukolsky, W. T. Vetterling, and B. P. Flannery. The Art of Scientific Computing, 29, (2007).

[68] A. Bellen and M. Zennaro, *OUP Cat.*, 2003.

[69] T. Erneux, Springer, (2008).

[70] G. Teschl, *Baylor.Edu*, 140, (2012).

[71] M. Conti and C. Turchetti. *IEEE Trans. Circuits Syst. I Fundam. Theory Appl.*, 41, 841–858, (1994).

[72] J. C. Sprott. *Am. J. Phys.*68, 758–763, (2000).

[73] R. Thepi Siewe, U. Simo Domguia and P. Woafo. Int. J. Nonlin. Sci and Num. Sim 19(2), 153-163, (2018)

[74] J. E. Marsden and M. McCracken, vol. 19. New York, NY: Springer New York, 1976.

[75] Aström KJ and Wittenmark B,Upper Saddle River NJ: Second edition Prentice-Hall, (1990).

[76] K. Srinivasan, D. V. Senthilkumar, K. Murali, M. Lakshmanan, and J. Kurths. Chaos 21,

023-119, (2011).

[77] T. Banerjee, D. Biswas. Conference paper I, (2011).

[78] T. Banerjee, D. Biswas, B.C. Sarkar. Nonlinear Dyn, DOI 10.1007/s11071-012-0490-3, (2012).

[79] D. Biswas, T. Banerjee. Nonlinear Dyn, DOI 10.1007/s11071-015-2484-4, (2012).

[80] T. Banerjee, D. Biswas, B. C. Sarkar. Conference Paper II, (2013).

[81] G. Habib, G. Rega, and G. Stepan, *J. Vib. Control*, (2014).

[82] G. Ablay, *Nonlinear Dyn.*, vol. 81, no. 4, pp. 1795–1804, (2015).

[83] R. Stratonovich, *Topic in the theory of random noise*. Gordon and Breach; New York, (1967)

[84] L. Graney and A. A. Richardson, *J. Comput. Appl. Math.*, vol. 7, no. 4, pp. 229–236, (1981)

[85] J. Li, W. Xu, X. Yang, and Z. Sun, *J. Sound Vib.*, vol. 309, no. 1, pp. 330–337, (2008).

[86] G. Ablay. Nonlinear Dyn. DOI 10.1007/s11071-015-2107-0, (2011)

[87] H. XiuJing and B. QinSheng, Sci. China.Technol. Sc., 55, 702-708, (2012).

[88] Alberto d'Onofrio, *Bounded noises in Physics, Biology and Engineering*. Springer Science Media, New York, (2013).

[89] Y. Zheng and L. Bao. Nonlinear Dyn., 80, 1521-1529, (2015).

[90] L. Makouo and P. Woafo, Chaos Solitons Fractals, 94, 95-101, (2017).

[91] Kiam Heong Ang, G. Chong, and Yun Li, vol. 13, no. 4, pp. 559–576, Jul. (2005).

[92] E. W. Chimi Kontchou, H. B. Fotsin and P. Woafo. Phys. Scr. 77, 045–001, (2008).

[93] L. L. Kovács, J. Kövecses, and G. Stépán, *Int. J. Non. Linear. Mech.*, vol. 43, no. 6, pp. 514–520, (2008).

[94] P. R. Nwagoum Tuwa and P. Woafo. J. Vib. Control. 1–10,doi:10.1177/1077546316674609, (2016).

[95] H. C. Liaw, B. Shirinzadeh, and J. Smith, *Sensors Actuators, A Phys.*, vol. 138, no. 1, pp. 194–202, (2007).

[96] G. Y. Gu and L. M. Zhu, *Rev. Sci. Instrum.*, vol. 85, no. 5, (2014).

[97] Nana B, Yamgoué S. B., Tchitnga R, Woafo P. Chaos Soliton Fractals 104, 18–27, (2017).

[98] R. Thepi Siewe, U. Simo Domguia, and P. Woafo. CNSNS. 69, 343–359, (2019).

[99] T. D. S. Hamilton, *Handbook of linear integrated electronics for research*. McGraw-Hill.

[100] 'https://www.microchip.com/wwwproducts/ProductCompare/PIC18F4550/PIC18F45K50'.

[101] 'https://www.microchip.com/wwwproducts/ProductCompare/PIC16F877/PIC16F87A7'.

[102] 'https://www.circuitstoday.com/microcontroller-atmega32-invention-history'.

[103] Nana B, Yamgoué S.B., Tchitnga R, Woafo P. Chaos Soliton Fractals 112, 14–23, (2018).

Publications list of the PhD Candidate

Publications of this thesis

1. **R. Thepi Siewe**, A. F. Talla and P. Woafo, Experimental synchronization of two Van der Pol oscillators with nonlinear and delayed unidirectional coupling. Int. J. Nonl. Sci. and Num. Sim.18 (6), 513-523, (2017).

2. **R. Thepi Siewe**, U. Simo Domguia and P. Woafo, Microcontroller control/synchronization of the dynamics of Van der Pol oscillators submitted to disturbances. Int. J. Nonl. Sci. and Num. Sim.19(2), 153-163, (2018).

Others publications

1. **R. Thepi Siewe**, A. F. Talla, P. Woafo, Response of a resonant tunnelling diode optoelectronic oscillator coupled to a nonlinear electrical circuit. IET Optoelectronics, 10(6), 205-210, (2016).

2. **R. Thepi Siewe,** U. Simo Domguia and P. Woafo. Generation of pulse-like and bursting-like oscillations from nonlinear systems using embedded technologies and applications to excite mechanical arms. Commun Nonlinear Sci Numer Simulat 69, 343–359, (2019).

3. H. Simo, **R. Thepi Siewe**, J. K. Dutt, P. Woafo, Effects of delay, noises and fractional order on the peaks in antiperiodic oscillations in Duffing oscillator. Ind. J. Phy, 1-11, (2019).